



Isotopic signatures of production and uptake of H₂ by soil

Q. Chen^{1,2}, M. E. Poppa¹, A. M. Batenburg^{1,3}, and T. Röckmann¹

¹Institute for Marine and Atmospheric research Utrecht, Utrecht University, Utrecht, the Netherlands

²Department of Atmospheric Sciences, University of Washington, Seattle, Washington, USA

³Department of Applied Physics, University of Eastern Finland, Kuopio, Finland

Correspondence to: Q. Chen (chenqjie@uw.edu)

Received: 17 April 2015 – Published in Atmos. Chem. Phys. Discuss.: 1 September 2015

Revised: 11 November 2015 – Accepted: 12 November 2015 – Published: 24 November 2015

Abstract. Molecular hydrogen (H₂) is the second most abundant reduced trace gas (after methane) in the atmosphere, but its biogeochemical cycle is not well understood. Our study focuses on the soil production and uptake of H₂ and the associated isotope effects. Air samples from a grass field and a forest site in the Netherlands were collected using soil chambers. The results show that uptake and emission of H₂ occurred simultaneously at all sampling sites, with strongest emission at the grassland sites where clover (N₂ fixing legume) was present. The H₂ mole fraction and deuterium content were measured in the laboratory to determine the isotopic fractionation factor during H₂ soil uptake (α_{soil}) and the isotopic signature of H₂ that is simultaneously emitted from the soil (δD_{soil}). By considering all net-uptake experiments, an overall fractionation factor for deposition of $\alpha_{\text{soil}} = k_{\text{HD}} / k_{\text{HH}} = 0.945 \pm 0.004$ (95 % CI) was obtained. The difference in mean α_{soil} between the forest soil 0.937 ± 0.008 and the grassland 0.951 ± 0.026 is not statistically significant. For two experiments, the removal of soil cover increased the deposition velocity (v_d) and α_{soil} simultaneously, but a general positive correlation between v_d and α_{soil} was not found in this study. When the data are evaluated with a model of simultaneous production and uptake, the isotopic composition of H₂ that is emitted at the grassland site is calculated as $\delta D_{\text{soil}} = (-530 \pm 40) \text{‰}$. This is less deuterium depleted than what is expected from isotope equilibrium between H₂O and H₂.

1 Introduction

H₂ is considered an alternative energy carrier to replace fossil fuels in the future. However, the environmental and climate impact of a potential widespread use of H₂ is still under assessment. Several studies suggested that the atmospheric H₂ mole fraction might increase substantially in the future due to the leakage during production, storage, transportation and use of H₂, which could significantly affect atmospheric chemistry (Schultz et al., 2003; Tromp et al., 2003; Van Ruijven et al., 2011; Warwick et al., 2004).

In the troposphere, H₂ has a mole fraction of about 550 parts per billion (ppb = nmol mol⁻¹) and a lifetime of around 2 years (Novelli et al., 1999; Price et al., 2007; Xiao et al., 2007; Pieterse et al., 2011; 2013). H₂ can affect atmospheric chemistry and composition in several ways. Firstly, it increases the lifetime of the greenhouse gas methane (CH₄) via its competing reaction with the hydroxyl radical (OH) (Schultz et al., 2003; Warwick et al., 2004). Additionally, H₂ affects air quality because it is an ozone (O₃) precursor and indirectly increases the lifetime of the air pollutant carbon monoxide (CO) through competition for OH. In the stratosphere, H₂O that is produced through the oxidation of H₂ increases humidity, which can result in increased formation of polar stratospheric clouds and O₃ depletion (Tromp et al., 2003), but this effect may be weaker than estimated initially (Warwick et al., 2004; Vogel et al., 2012).

The main sources of tropospheric H₂ are the oxidation of CH₄ and non-methane hydrocarbons (NMHC) (48 %), biomass burning (19 %), fossil fuel combustion (22 %) and biogenic N₂ fixation in the ocean (6 %) and on land (4 %), while the main sinks are soil uptake (70 %) and oxidation by OH (30 %) (Pieterse et al., 2013).

The biogenic soil sink of H₂ is the largest and most uncertain term in the global atmospheric H₂ budget. Conrad and Seiler (1981) assumed that the soil uptake of atmospheric H₂ is most likely due to consumption by abiotic enzymes, since there were no soil microorganisms known to be able to fix H₂ at the low atmospheric mole fraction at that time. This remained the basic hypothesis of many further soil uptake studies (Conrad et al., 1983; Conrad and Seiler, 1985; Ehhalt and Rohrer, 2011; Guo and Conrad, 2008; Häring et al., 1994; Smith-Downey et al., 2006). However, Constant et al. (2008a) were first to identify an aerobic microorganism (*Streptomyces* sp. PCB7) that can consume H₂ at tropospheric ambient mole fractions and suggested that active metabolic cells could be responsible for the soil uptake of H₂ rather than extracellular enzymes. Further studies showed that uptake activity at ambient H₂ level is widespread among the streptomycetes (Constant et al., 2010) and it was postulated that high-affinity H₂-oxidizing bacteria are the main biological agent responsible for the soil uptake of atmospheric H₂ (Constant et al., 2011). Khdhiri et al. (2015) suggested that the relative abundance of high-affinity H₂-oxidation bacteria and soil carbon content could be used as predictive parameters for the H₂-oxidation rate. Determining the dominant mechanism of the H₂ soil uptake activity is still an active area of research.

It has been shown that soil uptake of H₂ can coexist with soil production (Conrad, 1994). H₂ is produced in the soil during N₂ fixation (e.g., by bacteria living symbiotically in the roots of legumes such as clover or beans) and dark fermentation. Although the H₂ produced in the soil by, e.g., N₂ fixation can be largely consumed within the soil, a significant amount of H₂ escapes to the atmosphere (Conrad and Seiler, 1979, 1980). Conrad and Seiler (1980) estimated that 2.4 to 4.9 Tg a⁻¹ of H₂ is emitted into the atmosphere through N₂ fixation on land.

One approach to better understand the sources and sinks of H₂ is to investigate the isotopic fractionation processes involved, which act as a fingerprint for H₂ emitted from different sources or destroyed by different sinks. The isotopic composition of H₂ is expressed as

$$\delta(\text{D}, \text{H}_2) = \frac{R_{\text{sa}}}{R_{\text{VSMOW}}} - 1,$$

where R_{sa} is the D/H ratio of the sample H₂ and $R_{\text{VSMOW}} = (155.76 \pm 0.8)$ parts per million (ppm = mmol mol⁻¹) is the same ratio of the standard material, Vienna Standard Mean Ocean Water (VSMOW) (De Wit et al., 1980; Gonfiantini et al., 1993). For brevity, we will use the notation δD (= $\delta\text{D}(\text{D}, \text{H}_2)$) throughout the rest of this paper. The δD values are usually given in per mill (‰). Recent studies showed that the global mean δD value of atmospheric H₂ is about +130 ‰ (Batenburg et al., 2011; Gerst and Quay, 2000, 2001; Rice et al., 2010).

The HH molecule is consumed preferentially over HD during both OH oxidation and soil uptake, with OH oxidation

causing a much stronger isotope fractionation effect. Only a few studies have investigated the soil uptake of H₂ with isotope techniques. Gerst and Quay (2001) carried out field experiments in Seattle, USA, and found α_{soil} (= $k_{\text{HD}} / k_{\text{HH}}$) to be 0.943 ± 0.024 (1σ). Note that k_{HD} and k_{HH} are removal rate constants for HD and HH, respectively. Rahn et al. (2002a) collected air samples from four forest sites in ecosystems of different ages in Alaska, USA, in July 2001 and obtained a similar average value (0.94 ± 0.01). They suggested that α_{soil} depends on the forest maturity, with smaller fractionation for more mature forests. Since the more mature forests showed larger deposition velocity (v_{d}) of H₂, they further suggested that lower uptake rates involve greater isotopic fractionation (α_{soil} further from 1) than fast uptake rates. Rice et al. (2011) performed deposition experiments in Seattle and found α_{soil} varying from 0.891 to 0.976, with a mean of 0.934. They found α_{soil} to be correlated with v_{d} , with smaller isotope effects (α_{soil} closer to 1) occurring at higher v_{d} , which agreed with the suggestion by Rahn et al. (2002a). In addition, unpublished experiments from Rahn et al. (2005) yielded $\alpha_{\text{soil}} = 0.89 \pm 0.03$ in three upland ecosystems that were part of an Alaskan fire chronosequence. The data suggest that variability in the soil/ecosystem affects α_{soil} but no significant variability of α_{soil} with season was detected. Hitherto, only α_{soil} values from studies in Seattle and Alaska are available, and values from other locations and ecosystems are needed to learn more about the factors influencing α_{soil} .

The δD of H₂ from various surface sources has been reported as about -290 ‰ for biomass burning (Gerst and Quay, 2001; Haumann et al., 2013) and between -360 and -200 ‰ for fossil fuels combustion (Rahn et al., 2002b; Vollmer et al., 2012). So far no field studies have determined the isotopic composition of H₂ emitted from soil. Two laboratory studies examined the isotopic signature of H₂ produced from N₂ fixation. Luo et al. (1991) reported a fractionation factor $\alpha_{\text{H}_2/\text{H}_2\text{O}} = R(\text{D}/\text{H}, \text{H}_2) / R(\text{D}/\text{H}, \text{H}_2\text{O}) = 0.448 \pm 0.001$ between the H₂ produced from N₂ fixation and the H₂O used to grow the N₂-fixing bacteria for *Synechococcus* sp. and 0.401 ± 0.002 for *Anabaena* sp., respectively. Walter et al. (2012) reported $\alpha_{\text{H}_2/\text{H}_2\text{O}} = 0.363 \pm 0.019$ for the N₂-fixing rhizobacterium *Azospirillum brasiliensis*. It has been proposed that microbiological H₂ consumption and production could modify the thermal isotopic equilibrium between H₂ and H₂O in low-temperature hydrothermal fluids (Kawagucci et al., 2010). Compared to the surface sources, H₂ produced from CH₄ and NMHC oxidation is isotopically strongly enriched in deuterium, with δD between +120 and +180 ‰ (Rahn et al., 2003; Röckmann et al., 2003a; Pieterse et al., 2011).

Here we report measurements of the isotopic fractionation factors of H₂ during soil deposition at two different sites in the Netherlands, a forest and a grassland site. For the grassland site we also determine the apparent isotopic composition of H₂ that was simultaneously emitted from soil during the experiment.

2 Methods

2.1 Sampling

Air samples were collected from a soil chamber at two locations in the Netherlands (Fig. 1): a grass field around the Cabauw tall tower (51°58' N, 4°55' E) and a forest site near Speuld (52°13' N, 5°39' E). Two types of ground cover (grass with and without clover) were sampled at Cabauw, while three types of forest (Douglas fir, beech and spruce) were selected in Speuld. More information about the soil and vegetation type can be found in Beljaars and Bosveld (1997) for the Cabauw site and in Heij and Erisman (1997) for the Speuld site.

Flask samples were filled with air from a soil chamber, using a closed-cycle air sampler (Fig. 2). The soil chamber consisted of two parts: the chamber body with a metal base at the bottom that was inserted about 2 cm into the soil and a removable transparent lid with two connections for air sampling. The chamber had a height of 40 cm, an area of 570 cm² and a volume of 22.8 L; the air inside was mixed by a fan. The sampler could hold four flasks installed in series, which could be bypassed independently; the flow and pressure in the flasks were controlled. The air was dried using Mg(ClO₄)₂. After passing through the flasks the air was returned to the soil chamber, which kept the pressure inside the chamber approximately constant during sampling.

Air samples were collected from the chamber in 1 L glass flasks at 0, 10, 20 and 30 min after closing the chamber (time interval changed to 5 min in Speuld because of the faster uptake). The gas flasks (Normag, Ilmenau, Germany) were made of borosilicate glass 3.3 with O-ring-sealed stopcocks made of PCTFE (Kel-F) and covered with a dark hose. Thorough tests have demonstrated that air samples with typical trace gas content are stable in these flasks (Rothe et al., 2004). In the beginning, the whole sampling unit (all lines, connections and flasks) was flushed with ambient air for about 10 min at a flow rate of 2 L min⁻¹ and a pressure of 100 kPa, with all flasks open and the chamber lid open. This initial flushing process was designed to fill the flasks with background air. The air pressure inside the flasks was increased to 200 kPa (180 kPa for Speuld samples) by adjusting the flow control valve and the valves on two pressure gauges (Fig. 2) before chamber closing and then maintained constant during the whole sampling time. The flow rate was maintained at 2 L min⁻¹ at ambient pressure and temperature with a rotameter and the pressure inside the chamber was maintained at 100 kPa during the whole sampling time. The temperature was not recorded during the sampling. After the initial flushing, the first flask was closed and then the chamber was closed as well. Afterwards, the air was flushed from the chamber through three flasks (the first flask was bypassed) and back to the chamber. After 10, 20 and 30 min, the second, third and fourth flasks were closed.

A total of 36 sets of air samples were collected in Cabauw during summer (June, July and August) 2012 and 12 sets were collected in Speuld in September 2012. Each set contains four air samples. In total, 186 valid samples were analyzed for H₂ mole fraction and its deuterium content (six were lost during sampling, transportation and measurement). All the Speuld samples and about half of the Cabauw samples were further used for analysis in this study. The reason why 50 % of the Cabauw experiments were not used is that these experiments showed neither strong H₂ emission nor H₂ uptake and the isotopic signals were weak. Most experiments were conducted with the 22.8 L volume soil chamber as described above, while 10 experiments were conducted with a larger automated soil chamber with a volume of 125 L and a height of 22.5 cm.

2.2 Laboratory determination of H₂ mole fraction and deuterium content of air samples

The mole fraction and δD of H₂ were measured with a gas chromatography isotope ratio mass spectrometry (GC/IRMS) setup (Rhee et al., 2004). For H₂ mole fractions, the laboratory working standards are linked to the MPI-2009 scale (Jordan and Steinberg, 2011). The δD values of the laboratory reference gases are indirectly linked to mixtures of synthetic air with H₂ of known isotopic composition, certified by Messer Griesheim, Germany (Batenburg et al., 2011). Most of the samples collected from Cabauw were measured within 2 months after sampling, while the samples from Speuld were kept in a dark storage room for around 4 months before measurement.

The operational principle of the GC/IRMS system is to separate H₂ from the air matrix at low temperature (about 36 K) and measure the HH and HD content with a mass spectrometer. The measurement includes four main steps.

- A glass sample volume (750 mL) is evacuated and subsequently filled with sample air to approximately 700 mbar. This volume is then exposed to a cold head (36 K) of a closed-cycle helium compressor for 9 min. During this stage, all gases except H₂, helium (He) and neon (Ne) condense.
- The remainder in the headspace of the cold head and sample volume is then flushed with He carrier gas to a pre-concentration trap where H₂ is collected on a 25 cm long, 1/8 inch OD (outside diameter) stainless steel tube filled with fine grains (0.2 to 0.5 mm) of 5 Å molecular sieve, for 20 min. The pre-concentration trap is cooled down to the triple point of nitrogen (63 K) by keeping it in a liquid N₂ reservoir that is further cooled down by pumping on the gas phase.
- After the collection of H₂, the pre-concentration trap is warmed up to release the absorbed H₂, which is then cryo-focused for 4 min on a capillary (25 cm long,

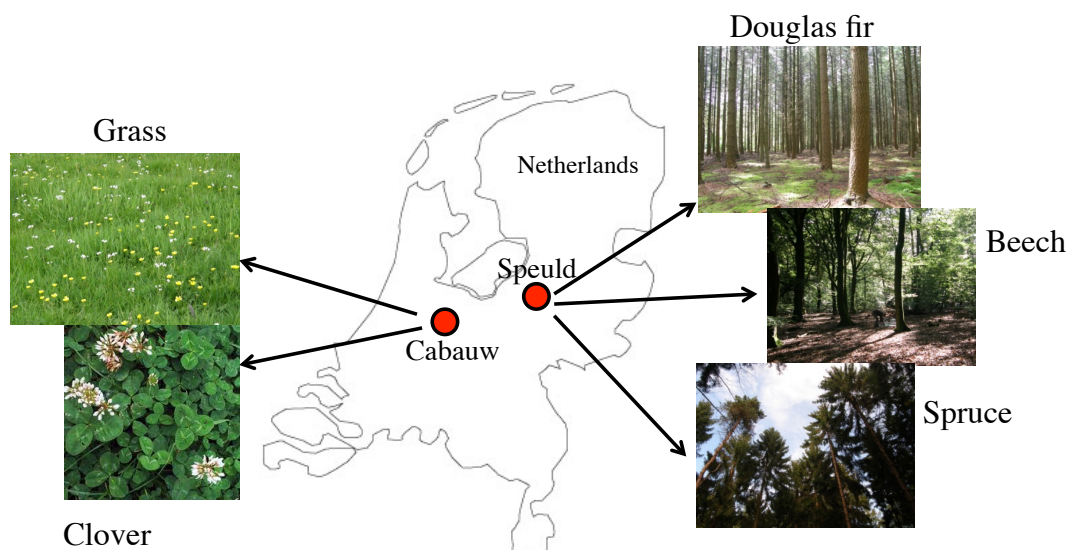


Figure 1. The location of the two sampling sites (Cabauw and Speuld) in the Netherlands, as well as the plant species there.

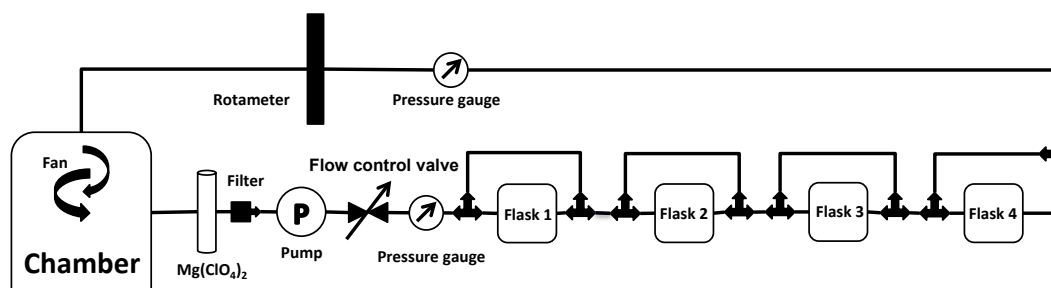


Figure 2. Scheme of the sampling setup using the closed-cycle air sampler. The volume of the soil chamber was 22.8 L and the volume of each flask was 1 L.

0.32 mm inside diameter) filled with 5 Å molecular sieve at 77 K. After that, the cryo-focus trap is warmed up to ambient temperature and the H₂ sample is flushed with He carrier gas onto the GC column (5 Å molecular sieve, ≈ 323 K) where H₂ is chromatographically purified from potential remaining interferences.

- In the end, the purified H₂ is carried by the He carrier gas via an open split interface (Röckmann et al., 2003b) into the IRMS for D / H ratio determination.

More details about the GC/IRMS system and measurement steps can be found in Rhee et al. (2004) and Röckmann et al. (2010). The data correction procedures and isotope calibration are similar to those described in Batenburg et al. (2011). Four reference gases were used to determine the δD values of the samples. Two of them (Ref-1 and Ref-2) with δD values of (+207.0 ± 0.3)‰ and (+198.2 ± 0.5)‰ were calibrated and used previously in Batenburg et al. (2011). The other two new reference gases (Ref-3 and Ref-4) were calibrated vs. Ref-1 and Ref-2. The δD value of Ref-3 was (−183 ± 2.4)‰. Ref-4 was a fre-

quently measured reference gas that was measured usually about five times per sequence of measurement, while other three reference gases were measured about one to three times per sequence of measurement. The δD value of Ref-4 dropped linearly with time from −115 to −157 ‰ between 1 June 2012 and 15 February 2013, while the other three reference gases were stable.

2.3 Non-linearity of the GC/IRMS system

Ideally, the δD of H₂ measured with the GC/IRMS should not depend on the total amount of H₂ used for analysis, but in practice a dependence of the isotopic composition on the amount of H₂ is observed for low mole fractions. This is called non-linear behavior, and it is a particularly severe limitation for soil uptake studies, since the mole fraction in such samples can decrease by more than an order of magnitude. For comparison, in ambient background air the H₂ mole fraction variations are usually no more than 20 %.

Experiments were carried out with different quantities of air from various laboratory reference bottles with known δD

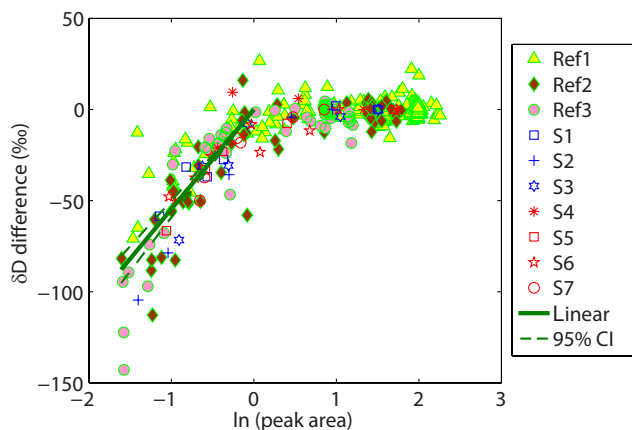


Figure 3. Difference of δD from the assigned value for different gases including reference gases (Ref1-3) and laboratory flask samples (S1-7). A linear function ($y = 54.6x$) was fit to the data with peak area between 0.2 and 1.0 Vs (green solid line; the dashed lines represent the 95 % confidence interval of the fit). This function was used to correct the soil experiment data that were measured at low peak areas.

to determine a suitable correction for the non-linear behavior. The measured δD increases with the mass 2 sample peak area, which is proportional to the H₂ quantity in the sample. In the peak area range of 0.2 Vs to 1 Vs this relation can be parameterized by a logarithmic function $\delta D = 54.6 \ln(\text{peak area (Vs)}^{-1}) \%$, which is used as correction function for the measurements at low peak areas (Fig. 3). The linearity correction introduces an additional uncertainty due to uncertainties in the logarithmic fit, particularly at low peak areas. The total assigned uncertainty for each measurement is calculated from the analytical and fitting uncertainty, as a function of peak area (Fig. 4). It is 2 % for $\ln(\text{peak area (Vs)}^{-1})$ of 1.5 or more (equivalent to more than 600 ppb H₂ in an air sample) but increases to 32 % when $\ln(\text{peak area (Vs)}^{-1})$ drops to -1.6 (≈ 20 ppb H₂ in air sample). In total, the δD results of 18 Speuld samples that were measured at these low peak areas were corrected with this linearity correction. Possible additional systematic errors (a few %) may arise from uncertainties in the initially assigned δD values of the commercial calibration gases, changes of these values in the process of creating calibration mixtures with near-ambient H₂ concentration, and the calibration measurements themselves (Batenburg et al., 2011).

2.4 Data evaluation

Assuming first order kinetics for H₂ removal and a constant production rate P over the course of a deposition experiment, the time evolution of the mole fraction c of non-deuterated H₂ (HH) inside the soil chamber can be expressed as

$$\frac{dc}{dt} = P - kc, \quad (1)$$

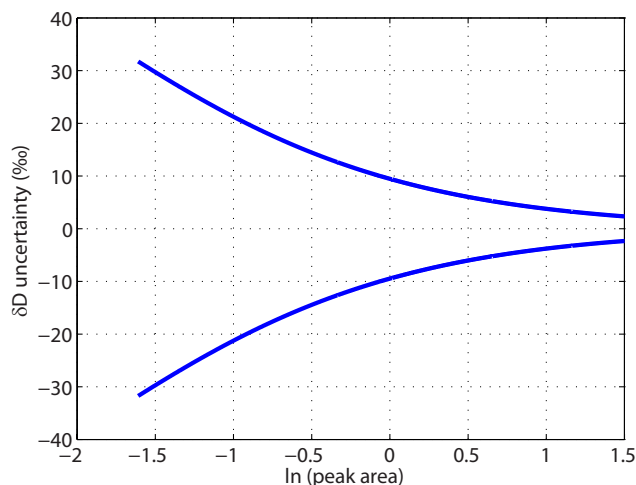


Figure 4. Calculated total assigned uncertainty of δD (consisting of analytical uncertainty and uncertainty arising from the linearity correction) for air samples with $\ln(\text{peak area})$ ranging from -1.6 to 1.5.

where k is the first order uptake rate constant of HH. For well-mixed air in the chamber, $k = v_d / h$, where v_d is the gross deposition velocity of H₂ and h is the chamber height. The gross deposition velocity is the deposition velocity corrected for production, which is different from the net deposition velocity reported in some studies in the past that showed the effective uptake of H₂ from the atmosphere. The solution of Eq. (1) is of the form

$$c = (c_i - c_e) e^{-kt} + c_e, \quad (2)$$

where c , c_i and $c_e (= P / k)$ are the mole fractions of HH at time t , initially and at equilibrium, respectively. Therefore, P and k can be obtained by fitting an exponential function to the time evolution of HH inside the chamber. Similarly, we can obtain P' and k' from the time evolution of HD.

$$c' = (c'_i - c'_e) e^{-k't} + c'_e, \quad (3)$$

where c' , c'_i , $c'_e (= P' / k')$, P' and k' are the corresponding parameters for HD.

Equations (2) and (3) constitute the mass balance model that we used to analyze our data. When k , k' , P and P' have been determined, α_{soil} and δD_{soil} can be calculated simply as

$$\alpha_{\text{soil}} = \frac{k'}{k} \quad (4)$$

$$\delta D_{\text{soil}} = \frac{P'/P}{2RV_{\text{SMOW}}} - 1. \quad (5)$$

However, fitting an exponential curve to only four sample data yields relatively large errors for k , k' , P and P' , which propagate to large errors for α_{soil} and δD_{soil} if they are determined directly from Eqs. (4) and (5).

In Rice et al. (2011), Eqs. (2) and (3) were combined to calculate α_{soil} in the presence of both source and sink of H₂ using c_e and c'_e from the exponential fits:

$$\ln \frac{c'_i - c'_e}{c'_i - c'_e} = \frac{k'}{k} \ln \frac{c - c_e}{c_i - c_e}. \quad (6)$$

$\alpha_{\text{soil}} = k'/k$ can be obtained by plotting $\ln \frac{c'_i - c'_e}{c'_i - c'_e}$ vs. $\ln \frac{c - c_e}{c_i - c_e}$ and fitting a linear function. In the absence of soil emission ($c_e = c'_e = 0$), Eq. (6) collapses to the well-known Rayleigh fractionation equation that is used to quantify the isotope fractionation during single stage removal processes in the absence of sources.

For the high emission measurements, where production overwhelms consumption, we use the relations $c_e = P/k$ and $c'_e = P'/k'$ and obtain P'/P from the slope of $c'_e \ln \frac{c'_i - c'_e}{c'_i - c'_e}$ against $c_e \ln \frac{c - c_e}{c_i - c_e}$. Then δD_{soil} is calculated from Eq. (5).

2.5 Flask sampling model

The advantage of sampling with the soil chamber system described in Sect. 2.1 was that the pressure in the soil chamber stayed constant even when several large samples (2 L each) were taken. A disadvantage was that the volume of air inside the flasks (8 L of air in total) was considerable compared to the volume of air inside the soil chamber (22.8 L). This had two effects: (1) a significant part of the air was at each time separated from the chamber and thus from the soil production and uptake and, (2) because of the time lag to flush the samples, the air in a flask was not the same as the air in the chamber at the same time.

We built a flask sampling model to derive correction factors that take into account the influence of the flask sampling system. For a given combination of uptake and production rates, the model simulates the evolution of the H₂ mole fraction in two configurations: the soil chamber alone and the soil chamber plus four flasks as in our experiments. The model is described in detail in Appendix A. An example of a simulation is shown in Fig. 5. Compared to the situation without flasks, there is a time lag in the decay of H₂ for both the chamber and the flasks after introducing four flasks in the model. The time lag for the second flask is about 2.5 min. It increases to 5 min for the third flask and is even longer for the fourth flask.

It is obvious that the sampling process strongly affects the uptake rate k_{app} and production rate P_{app} obtained from the direct flask measurements, so we corrected all k_{app} and P_{app} values with the correction coefficients derived from this flask sampling model (Appendix A). For a fixed chamber volume, sample pressure, flow rate and time interval of the flask collection that are all recorded for each experiment, the relationship between the actual uptake rate constant k_{true} and apparent uptake rate constant k_{app} can be obtained (see Appendix A). Under the same sampling conditions for a fixed

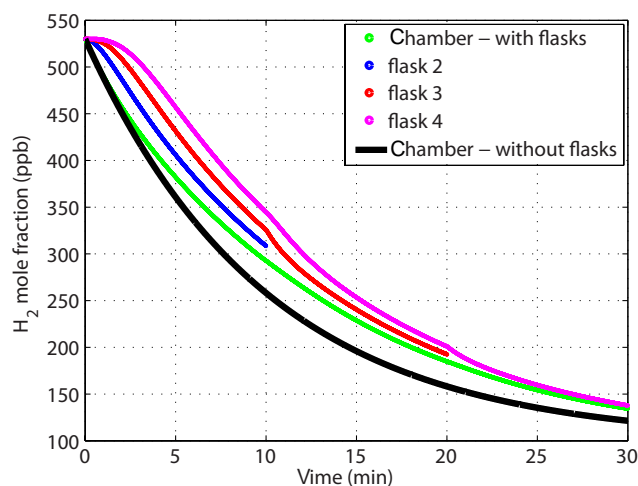


Figure 5. Results of the flask sampling model with the following parameters: $k = 0.1 \text{ min}^{-1}$, $P = 10 \text{ ppb min}^{-1}$ and $c_1(t = 0) = 530 \text{ ppb}$. The figure shows the evolution of H₂ mole fraction in the chamber (green curve), in flask 2 (blue curve), flask 3 (red curve) and flask 4 (magenta curve) as a function of time and what would be expected for a chamber without flasks (black curve). Flask 1 was closed before closing the chamber (at time 0 when all volumes contained the same air).

value of P_{app} , the relationship between actual production rate P_{true} and apparent production rate P_{app} depends on k_{true} (Fig. 10b).

To evaluate the data, we first applied an exponential fit as in Eq. (2) to the measured HH mole fractions for the four flasks in each experiment and obtained apparent values k_{app} , P_{app} and $c_{e,\text{app}}$ from the fit parameters. Then we used the correction factors derived from the flask sampling model to retrieve true values k_{true} and P_{true} from the apparent values k_{app} and P_{app} . One can obtain k'_{true} and P'_{true} by applying the same method to HD mole fractions inside four flasks.

To determine α_{soil} , we plotted $\ln \frac{c'_i - c'_{e,\text{app}}}{c'_i - c'_{e,\text{app}}}$ vs. $\ln \frac{c - c_{e,\text{app}}}{c_1 - c_{e,\text{app}}}$ (Eq. 6, Fig. 7) and obtained $\alpha_{\text{soil,app}}$ from the slope of the linear regression. Here, c and c' are HH and HD mole fractions in each of the four flasks; c_1 and c'_1 are HH and HD mole fractions of the first flask; $c_{e,\text{app}}$ and $c'_{e,\text{app}}$ are apparent HH and HD equilibrium mole fractions obtained from the exponential fits of HH and HD mole fractions inside the four flasks. We determined the relationship (Fig. 10c) between $\alpha_{\text{soil,true}}$ and $\alpha_{\text{soil,app}}$ obtained from $\ln \frac{c'_i - c'_{e,\text{app}}}{c'_i - c'_{e,\text{app}}}$ vs. $\ln \frac{c - c_{e,\text{app}}}{c_1 - c_{e,\text{app}}}$ using the flask sampling model (see Appendix A1.3). The correction coefficients for each experiment are given in Table 3.

Similarly, we obtained $P'_{\text{app}}/P_{\text{app}}$ by plotting $c'_{e,\text{app}} \ln \frac{c'_i - c'_{e,\text{app}}}{c'_i - c'_{e,\text{app}}}$ vs. $c_{e,\text{app}} \ln \frac{c - c_{e,\text{app}}}{c_1 - c_{e,\text{app}}}$ (Fig. 9), and calculated $\delta D_{\text{soil,app}}$ by use of Eq. (5). Then we retrieved $\delta D_{\text{soil,true}}$ by use of the flask sampling model (Fig. 10d). The corresponding correction coefficients for $\delta D_{\text{soil,app}}$ for each net-emission experiment are shown in Table 3. More

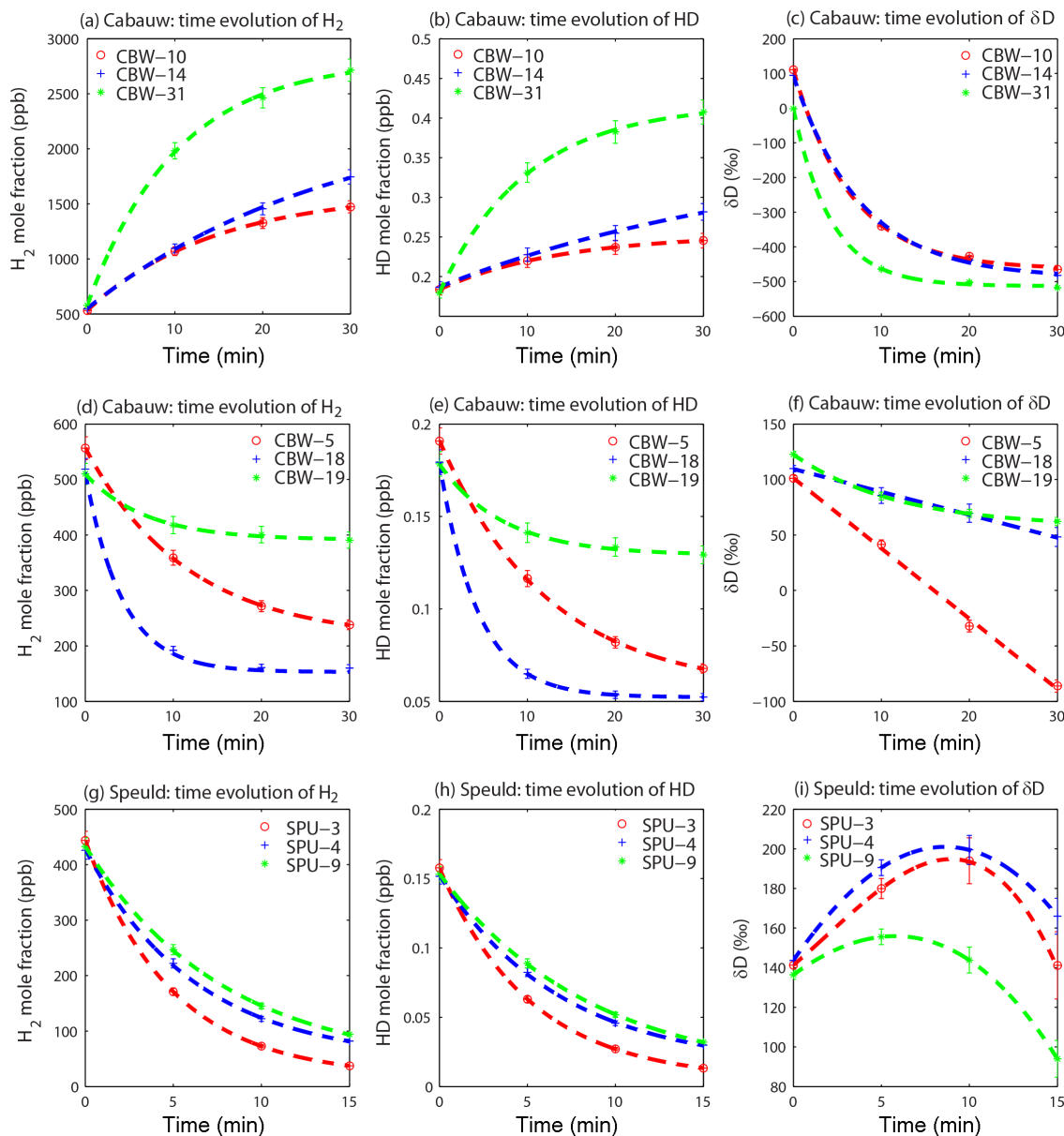


Figure 6. Time evolution of H₂, HD and δD in Cabauw (upper and middle panels) and in Speuld (lower panel) for representative experiments. HD is calculated from H₂ and δD . The H₂ data are fitted with an exponential function of the form $c = (c_1 - c_{e,app})e^{-k_{app}t} + c_{e,app}$, where c_1 and $c_{e,app}$ are the H₂ mole fractions initially and in equilibrium, and k_{app} is the apparent soil uptake rate constant for H₂. A similar exponential function is applied to the HD data. Error estimates for H₂, HD and δD are shown. The connecting lines for δD data are included to guide the eye.

information about the retrievals of $\alpha_{soil,true}$ and $\delta D_{soil,true}$ can be found in Appendix A.

Overall, the sampling effect on δD_{soil} is small (less than 22 ‰). This means that the flask sampling system strongly affects the temporal evolution of HH and HD individually (Fig. 5), and the uptake and production rates derived from flask measurements, but the effects on the computed isotopic signature of the source and sink are relatively small. More de-

tails and discussion of the flask sampling model corrections are provided in Appendix A.

3 Results

3.1 Temporal evolution of H₂, HD and δD

Figure 6 shows examples for the temporal evolution of H₂, HD and δD in Cabauw and Speuld, with error estimates in-

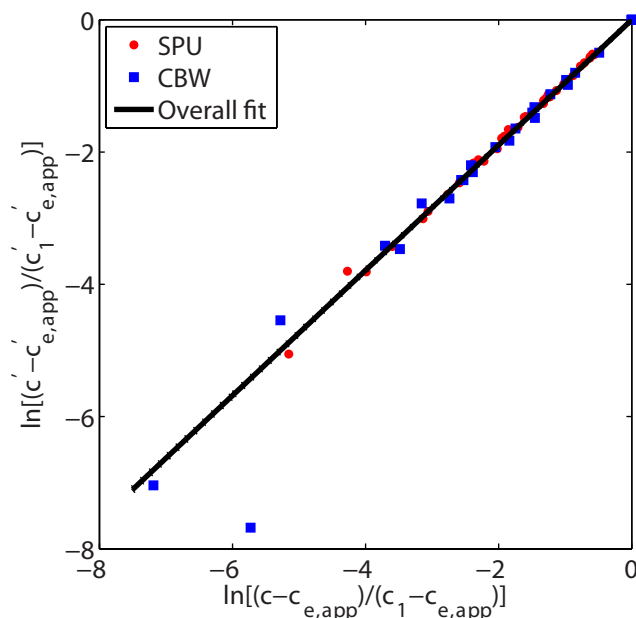


Figure 7. Plot of $\ln \frac{c' - c'_{e,app}}{c_1 - c'_{e,app}}$ vs. $\ln \frac{c - c_{e,app}}{c_1 - c_{e,app}}$ for all Speuld and Cabauw net-uptake experiments. The slope of the linear fit to the data returns the fractionation factor $\alpha_{\text{soil},app} = 0.947 \pm 0.004$ (95 % CI). Errors in x and y direction for each data point were considered. One outlier (“CBW-18”) was not included in the fitting. The 95 % confidence intervals of the fit line are included as dashed lines but largely overlap with the fit line.

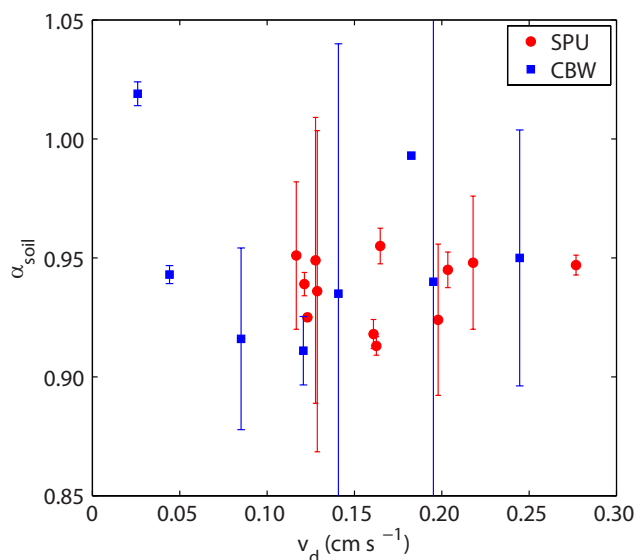


Figure 8. Correlation between α_{soil} and v_d for all Speuld experiments and Cabauw net-uptake experiments. The errors for α_{soil} were taken from Table 1.

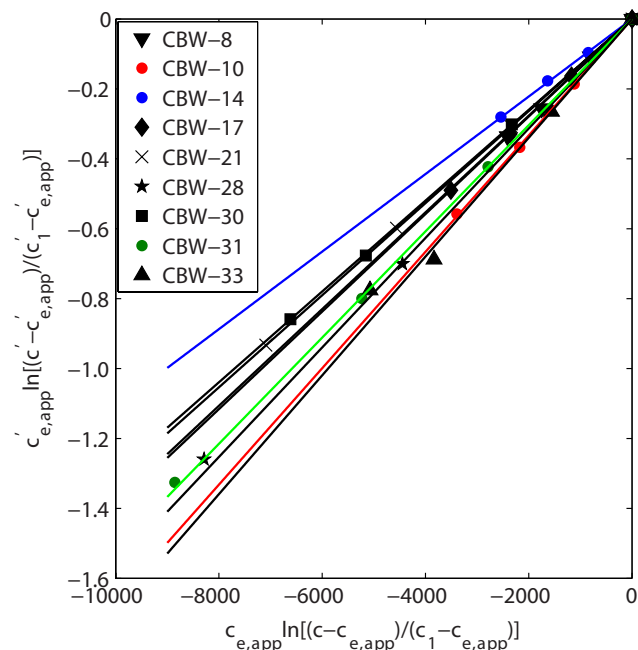


Figure 9. Plot of $c'_{e,app} \ln \frac{c' - c'_{e,app}}{c_1 - c'_{e,app}}$ vs. $c_{e,app} \ln \frac{c - c_{e,app}}{c_1 - c_{e,app}}$ for nine Cabauw net-emission experiments. A linear function was fit to each individual data set and the slope was used to calculate the $\delta D_{\text{soil},app}$ value for each experiment. Errors in x and y direction for each data point were considered.

cluded. The errors for H₂ and HD are about 4 % of the respective mole fraction. The error for δD ranges from 2 to 17 %.

Some of our Cabauw experiments show net soil emission of H₂ (upper panels) and some show net soil uptake (middle panels), while all Speuld experiments show net uptake of H₂ (lower panels). In the Cabauw net-emission experiments, the increase in H₂ mole fractions is associated with a strong decrease in δD , showing a strongly depleted H₂ source. However, the net-uptake experiments at Cabauw show also a decrease in δD , albeit smaller. In the Speuld experiments, the uptake of H₂ is much faster; the δD increases in the beginning but then decreases again towards the end of the sampling, when the H₂ mole fractions are low.

As mentioned in the introduction, soil uptake tends to increase δD while soil emission tends to decrease δD of H₂. The continuous decrease of δD with time in all Cabauw experiments and the eventual decrease of δD in all Speuld experiments clearly show that there is concurrent soil emission even with net uptake. Thus, the equilibrium H₂ concentration in our experiments is not just a threshold concentration where microbial uptake stops, but the isotopic evolution shows that there is an active overlapping emission (Conrad, 1994).

Table 1. The deposition velocity (v_d), fractionation factor (α_{soil}) as well as its error estimate and soil cover information for each Speuld experiment (a) and Cabauw net-uptake experiment (b). The SD represents standard deviation and SE represents standard error. The errors of α_{soil} represent the 95 % confidence interval (CI) for $\alpha_{\text{soil,app}}$ obtained from $\ln \frac{c' - c'_{e,app}}{c'_1 - c'_{e,app}}$ vs. $\ln \frac{c - c_{e,app}}{c_1 - c_{e,app}}$.

(a)	F_n (nmol m ⁻² s ⁻¹)	v_d (cm s ⁻¹)	α_{soil}	Error α_{soil}	Soil cover
SPU-1	-30.1	0.20	0.924	0.032	D. fir, moss
SPU-2	-35.3	0.22	0.948	0.028	D. fir, needles
SPU-3	-37.7	0.20	0.945	0.008	D. fir, moss
SPU-4	-26.1	0.16	0.913	0.004	D. fir, moss
SPU-5	-24.9	0.16	0.918	0.006	D. fir, moss
SPU-6	-13.2	0.12	0.951	0.031	D. fir, moss
SPU-7	-19.6	0.12	0.939	0.005	beech, leaves
SPU-8	-28.4	0.16	0.955	0.008	same subsite as SPU-7, leaves removed
SPU-9	-20.4	0.12	0.925	0.002	beech, leaves
SPU-10	-22.3	0.13	0.949	0.060	spruce, moss
SPU-11	-19.4	0.13	0.936	0.068	spruce, needles
SPU-12	-40.5	0.28	0.947	0.004	same subsite as SPU-11, needles removed
MEAN	-26.5	0.17	0.937	-	-
SD	8.2	0.05	0.014	-	-
SE	2.4	0.01	0.004	-	-
(b)	F_n (nmol m ⁻² s ⁻¹)	v_d (cm s ⁻¹)	α_{soil}	Error α_{soil}	Soil cover
CBW-5	-6.6	0.04	0.943	0.004	few clover, grass
CBW-7	-3.1	0.03	1.019	0.005	few clover, grass
CBW-16	-22.9	0.18	0.993	0.001	bare soil, few grass
CBW-18	-39.3	0.24	0.950	0.054	grass
CBW-19	-7.4	0.14	0.935	0.105	grass
CBW-20	-14.9	0.20	0.940	0.260	bare soil
CBW-25	-8.0	0.12	0.911	0.014	clover, grass
CBW-26	-6.1	0.09	0.916	0.038	grass
MEAN	-13.6	0.13	0.951	-	-
SD	12.2	0.08	0.037	-	-
SE	4.3	0.03	0.013	-	-

3.2 Emission and uptake strength of H₂

The production rate $P = P_{\text{true}}$ and uptake rate constant $k = k_{\text{true}}$ were obtained by applying exponential fits to the temporal evolution of H₂ and applying the corrections derived from the flask sampling model (Appendix A) to the P_{app} and k_{app} obtained from the exponential fits (Fig. 6). The deposition velocity (v_d), production flux (F_p), initial uptake flux (F_u) and net flux at the beginning of the experiment (F_n) were then calculated as follows:

$$v_d = kh, \quad (7)$$

$$F_p = \frac{Ph}{V_M}, \quad (8)$$

$$F_u = \frac{kc_1h}{V_M}, \quad (9)$$

$$F_n = F_p - F_u, \quad (10)$$

where h , V_M and c_1 are the chamber height, standard molar volume ($= 22.4 \text{ L mol}^{-1}$) and H₂ mole fraction of the first flask, respectively. We note that with our method we derive v_d as deposition velocity for the gross uptake, unlike most of the results reported in the literature that just measured net uptake.

The strongest soil uptake occurs in the Speuld experiments (Table 1a), with a mean v_d of (0.17 ± 0.02) (2 SE, $n = 12$) cm s⁻¹ (SE represents standard error). On average, the Cabauw experiments show weaker soil uptake, with a mean v_d of (0.13 ± 0.06) (2 SE, $n = 8$) cm s⁻¹ for the net-uptake experiments (Table 1b) and (0.06 ± 0.03) (2 SE, $n = 9$) cm s⁻¹ for the net-emission experiments (Table 2). In terms of the net H₂ flux F_n , this is (-26.5 ± 4.8) (2 SE, $n = 12$) nmol m⁻² s⁻¹ for Speuld experiments (Table 1a), (-13.6 ± 8.6) (2 SE, $n = 8$) nmol m⁻² s⁻¹ for Cabauw net-uptake experiments (Table 1b) and (49.5 ± 29.8) (2 SE, $n = 9$) nmol m⁻² s⁻¹ for Cabauw net-emission experiments

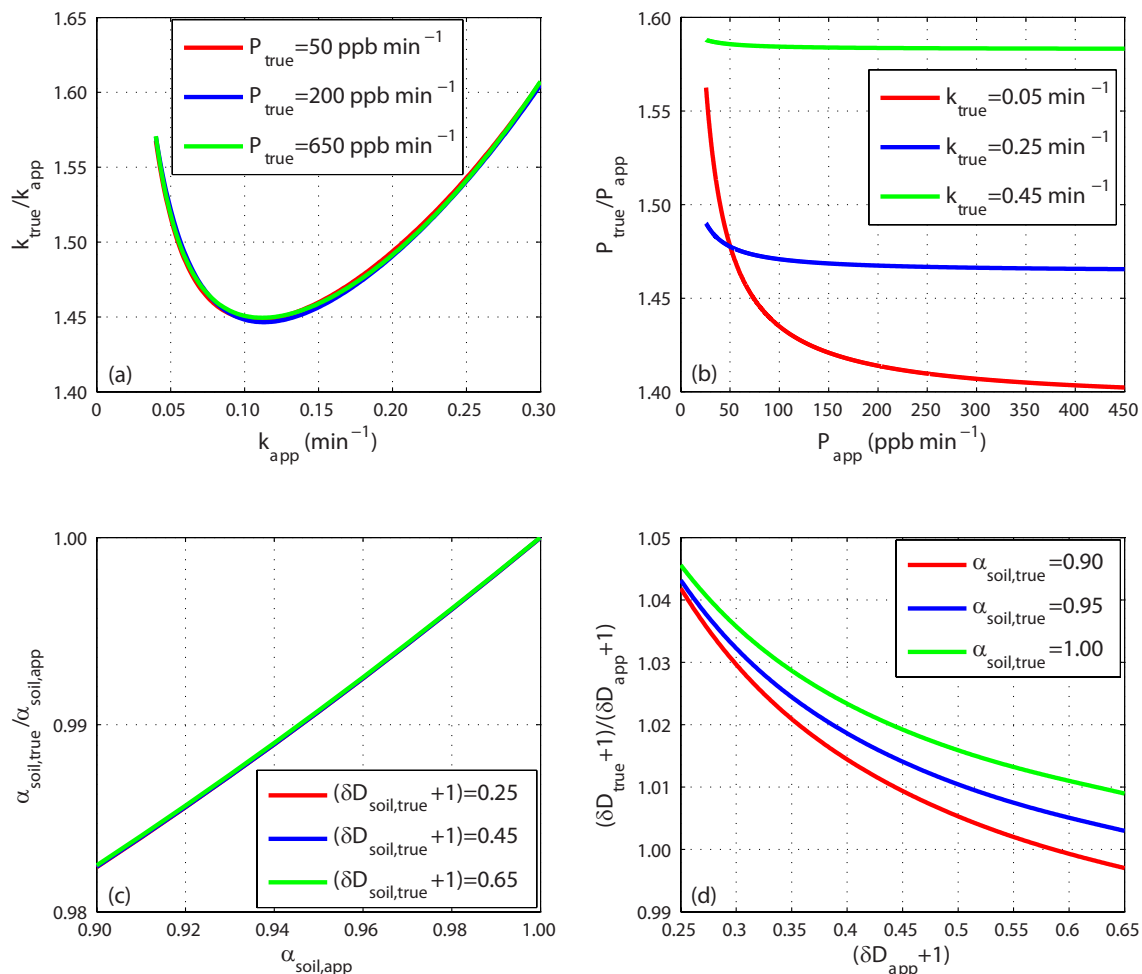


Figure 10. (a) The relationship between $k_{\text{true}}/k_{\text{app}}$ and k_{app} for P_{true} of 50, 200 and 650 ppb min^{-1} ; (b) between $P_{\text{true}}/P_{\text{app}}$ and P_{app} for k_{true} of 0.05, 0.25 and 0.45 min^{-1} ; (c) between $\alpha_{\text{soil,true}}/\alpha_{\text{soil,app}}$ and $\alpha_{\text{soil,app}}$ for $(\delta D_{\text{soil,true}}+1)$ of 0.25 to 0.65 for $k_{\text{true}} = 0.25 \text{ min}^{-1}$ and $P_{\text{true}} = 50 \text{ ppb min}^{-1}$; (d) between $(\delta D_{\text{soil,true}}+1)/(\delta D_{\text{soil,app}}+1)$ and $(\delta D_{\text{soil,app}}+1)$ for $\alpha_{\text{soil,true}}$ of 0.90 to 1.00 for $k_{\text{true}} = 0.25 \text{ min}^{-1}$ and $P_{\text{true}} = 50 \text{ ppb min}^{-1}$. The parameters of the sampling setup are $V' = 22.8 \text{ L}$, $f = 2 \text{ L min}^{-1}$, $\Delta t = 10 \text{ min}$ and the pressures inside the flasks and chamber are 200 and 100 kPa, respectively.

(Table 2), indicating strong uptake, weaker uptake and strong emission of H₂, respectively.

3.3 Fractionation during soil uptake

Soil uptake and soil emission have opposite effects on the isotopic composition of H₂ and can partly cancel each other. This will lead to additional uncertainty and we expect to obtain the most robust fractionation factor for soil uptake when the soil uptake is larger than the soil emission (Table 1a, b).

The resulting α_{soil} for Speuld (Table 1a) varies from 0.913 to 0.955, with a mean value of 0.937 ± 0.008 (2 SE, $n = 12$). Error estimates for HH and HD mole fraction at time t and at equilibrium are considered for the final error estimates of α_{soil} for each experiment.

Table 1b shows α_{soil} of the Cabauw net-uptake experiments. It should be noted that the soil-emitted H₂ interferes

much more with the fractionation during uptake in these Cabauw net-uptake experiments than in the Speuld experiments, which is illustrated by the consistent decrease in δD in the middle panel of Fig. 6. The derived values for α_{soil} vary from 0.911 to 1.019 with a mean value of 0.951 ± 0.026 (2 SE, $n = 8$) for these eight selected Cabauw net-uptake experiments. Both the mean and the standard error are higher than in the Speuld experiments (0.937 ± 0.008), but the difference is not significant at the 0.1 confidence level.

To graphically illustrate the calculation of α_{soil} with the mass balance model, we plot $\ln \frac{c' - c_{e,\text{app}}}{c'_1 - c_{e,\text{app}}}$ vs. $\ln \frac{c - c_{e,\text{app}}}{c_1 - c_{e,\text{app}}}$ for all Speuld and Cabauw net-uptake experiments in Fig. 7. A linear fit is applied to all the data and the overall $\alpha_{\text{soil,app}}$ is found to be 0.947 ± 0.004 (95 % CI). Applying a correction factor is not straightforward now because this analysis combines the results from different experiments. If we use the

Table 2. Net flux, deposition velocity and δD_{soil} (including error) obtained from the mass balance model for the net H₂ emission experiments.

Net emission	F_n (nmol m ⁻² s ⁻¹)	v_d (cm s ⁻¹)	δD_{soil} (‰)	Error δD_{soil} (‰)
CBW-8	24.5	0.05	-535	53
CBW-10	16.1	0.03	-460	17
CBW-14	13.7	0.02	-629	21
CBW-17	20.3	0.03	-542	1
CBW-21	42.0	0.04	-574	3
CBW-28	150.2	0.14	-488	83
CBW-30	41.0	0.05	-580	7
CBW-31	92.0	0.09	-509	7
CBW-33	46.2	0.10	-451	52
MEAN	49.5	0.06	-530	-
SD	44.7	0.04	59	-
SE	14.9	0.01	20	-

average of $\alpha_{\text{soil,true}} / \alpha_{\text{soil,app}}$ ratios (0.998) for all net-uptake experiments in Table 3 as the correction coefficient for this overall $\alpha_{\text{soil,app}}$, the overall α_{soil} is 0.945 ± 0.004 (95 % CI).

Figure 8 shows α_{soil} as a function of v_d for all Speuld experiments and Cabauw net-uptake experiments. The R^2 value is nearly 0 and the p value is 0.53 for the linear regression of all experiments, so no significant correlation between α_{soil} and v_d is found. Also, no significant correlation is found when considering the Speuld and Cabauw net-uptake experiments separately.

3.4 Isotopic signature of H₂ emitted from soil

As discussed in Sect. 2.4, the isotopic signature of H₂ emitted from the soil (δD_{soil}) can be obtained from the mass balance model. In order to minimize the influence of soil uptake on the computed δD_{soil} and obtain the most robust result, we only consider the Cabauw experiments with strong soil emission and weak soil uptake ($c_{\text{e,app}} > 1500$ ppb). In total, nine Cabauw experiments are selected (Table 2) and a linear fit is applied to the plot of $c'_{\text{e,app}} \ln \frac{c'_{\text{e,app}}}{c'_1 - c'_{\text{e,app}}}$ vs. $c_{\text{e,app}} \ln \frac{c - c_{\text{e,app}}}{c_1 - c_{\text{e,app}}}$ for each experiment (Fig. 9). It can be seen that the linear function fits the data very well for each experiment. The slope of the linear fit yields $P'_{\text{app}} / P_{\text{app}}$. This $P'_{\text{app}} / P_{\text{app}}$ ratio is used to calculate $\delta D_{\text{soil,app}}$ (Eq. 5). After correcting for the flask sampling effects (see Appendix A), the corresponding δD_{soil} values are shown in Table 2. The δD_{soil} value ranges from -629 to -451 ‰, with a mean value of (-530 ± 40) ‰ (2 SE, $n = 9$), which is very D depleted, but still considerably enriched relative to the value around -700 ‰ expected for thermodynamic equilibrium between H₂ and H₂O (Bottinga, 1969).

4 Discussion

4.1 Emission and uptake strength of H₂

The deposition velocity v_d is a measure of the strength of soil uptake. Both microbial removal and diffusion can affect v_d , and they can both be influenced by the temperature and moisture content of the soil (Ehhalt and Rohrer, 2013a, b). On average, the v_d obtained in this study is larger in the forest region (Table 1a) than in the grass/clover region (Table 1b and 2), in agreement with the conclusion from Ehhalt and Rohrer (2009).

The v_d of (0.06 ± 0.03) cm s⁻¹ found in our Cabauw net-emission experiments (Table 2) is similar to those reported in Conrad and Seiler (1980) (0.07 cm s⁻¹, both grass and clover) and Gerst and Quay (2001) (0.04 cm s⁻¹, grass), while the v_d of (0.13 ± 0.06) cm s⁻¹ in Cabauw net-uptake experiments (Table 1b) is larger than those studies with similar soil cover but close to values of 0.12 to 0.14 cm s⁻¹ found in savanna soil (Conrad and Seiler, 1985). The stronger soil uptake in Speuld forest ((0.17 ± 0.02) cm s⁻¹) agrees well with the beech forest results (0.06 to 0.22 cm s⁻¹) in Förstel (1988) and Förstel and Führ (1992). However, other studies at forest sites cited in Ehhalt and Rohrer (2009) showed lower v_d than our Speuld results. We note here that the v_d values reported in Conrad and Seiler (1980, 1985) were gross deposition velocities while those reported in Gerst and Quay (2001) were net deposition velocities. The specific method used to obtain v_d was not documented in the other studies. v_d values obtained from our experiments are gross deposition velocities.

The net-uptake flux F_n in our Speuld experiments and Cabauw net-uptake experiments is much larger than those found in Smith-Downey et al. (2008). They found a F_n of about -8 nmol m⁻² s⁻¹ for the forest, desert and marsh, which was similar to that for loess loamy soil in Schmitt et al. (2009). Our results are within the F_n range found in the mixed wood plains by Constant et al. (2008b) and the Harvard forest by Meredith (2012). Previously at our Cabauw site, Popa et al. (2011) obtained a F_n of only -3 nmol m⁻² s⁻¹ by using the radon tracer method. However, the Cabauw net-uptake experiments used for this evaluation were from selected places where uptake was strong, while the results in Popa et al. (2011) represented the overall uptake in the footprint of the Cabauw site, which is a much larger area (tens of km²).

Khdhiri et al. (2015) performed microbiological analyses on soil samples from the Cabauw and Speuld sites in order to find the drivers of soil H₂ uptake. They observed that the H₂ uptake rate under standard incubation conditions was significantly lower for the Cabauw soil samples than for the Speuld ones, which is consistent with our findings. The main factors that explained the differences were the relative abundance of high-affinity H₂-oxidizing bacteria and the soil carbon content, both lower on average for the Cabauw site.

Table 3. Sampling information and the correction coefficients ($k_{\text{true}}/k_{\text{app}}$, $P_{\text{true}}/P_{\text{app}}$, $\alpha_{\text{soil,true}}/\alpha_{\text{soil,app}}$ and $(\delta D_{\text{soil,true}}+1)/(\delta D_{\text{soil,app}}+1)$) used for each experiment. Size S refers to small chamber and size L refers to large chamber.

Exp.	Pressure (kPa)	Flow rate (L min ⁻¹)	Size	Δt (min)	k_{app} (min ⁻¹)	P_{app} (ppb min ⁻¹)	$k_{\text{true}}/k_{\text{app}}$	$P_{\text{true}}/P_{\text{app}}$	$\alpha_{\text{soil,true}}/\alpha_{\text{soil,app}}$	$(\delta D_{\text{soil,true}}+1)/(\delta D_{\text{soil,app}}+1)$
SPU-1	200	2	S	10	0.199	4.12	1.494	1.601	0.984	–
SPU-2	200	2.2	S	5	0.206	0.67	1.589	7.472	0.998	–
SPU-3	200	3.1	S	5	0.204	3.58	1.496	2.475	0.999	–
SPU-4	200	2.8	S	5	0.160	7.51	1.526	2.136	1.004	–
SPU-5	200	2.6	S	5	0.156	4.16	1.546	2.759	1.004	–
SPU-6	160	3.2	L	5	0.232	7.61	1.184	1.446	0.999	–
SPU-7	160	3.2	S	5	0.128	5.40	1.418	2.264	1.006	–
SPU-8	160	2.5	S	5	0.172	4.23	1.438	2.381	1.001	–
SPU-9	160	2.8	S	5	0.128	4.56	1.440	2.513	1.007	–
SPU-10	180	2.7	S	5	0.128	–	1.502	/	1.005	–
SPU-11	160	2.2	S	5	0.130	–	1.490	/	1.006	–
SPU-12	180	2.3	S	5	0.272	11.30	1.529	1.720	0.994	–
CBW-5	200	2	L	10	0.086	18.24	1.204	1.248	1.001	–
CBW-7	200	1.9	L	10	0.048	11.57	1.260	1.361	0.999	–
CBW-16	210	2.1	S	10	0.183	45.21	1.498	1.505	0.999	–
CBW-18	200	2	S	10	0.240	38.07	1.532	1.527	0.986	–
CBW-19	200	2	S	10	0.145	56.69	1.457	1.463	0.991	–
CBW-20	200	2	S	10	0.196	65.81	1.491	1.494	0.988	–
CBW-25	200	2	S	10	0.122	44.85	1.449	1.460	0.994	–
CBW-26	200	2	S	10	0.088	31.05	1.452	1.475	1.002	–
CBW-8	200	2	S	10	0.044	82.92	1.542	1.438	–	1.048
CBW-10	200	2.6	L	10	0.069	111.00	1.177	1.152	–	1.010
CBW-14	200	2.5	L	10	0.035	82.53	1.251	1.166	–	1.042
CBW-17	220	2.1	L	10	0.047	117.40	1.268	1.198	–	1.024
CBW-21	220	2	L	10	0.078	232.20	1.209	1.179	–	1.008
CBW-28	175	1.8	S	10	0.146	440.90	1.412	1.402	–	1.018
CBW-30	200	2	L	10	0.090	237.70	1.202	1.180	–	1.008
CBW-31	200	2	S	10	0.098	275.10	1.451	1.422	–	1.007
CBW-33	200	2	S	10	0.107	166.50	1.449	1.430	–	1.007

The emission of H₂ from the soil is large for the Cabauw net-emission experiments, with F_n ranging from 13.7 to 150.2 nmol m⁻² s⁻¹ and a median value of 41.0 nmol m⁻² s⁻¹ (Table 2). One experiment, “CBW-28”, shows unusually high emission, with H₂ increasing to 3010 ppb within 30 min. In comparison, Conrad and Seiler (1980) found a F_n of 23–32 nmol m⁻² s⁻¹ for a clover field. Except for the experiments “CBW-28” and “CBW-31”, our Cabauw net-emission experiments are close to the F_n found by them. The variability in F_n could be attributed to different N₂ fixation flux in our experiments, which could be affected by both spatial density of N₂ fixation organisms and their N₂ fixation activities. The N₂ fixation activity could be regulated by various factors including temperature, moisture, light availability and carbon storage (Belnap, 2001), which were not measured are therefore not discussed here.

4.2 Fractionation during soil uptake

Fractionation during soil uptake of H₂ can happen during the diffusion into the soil and due to microbial removal within the soil. To further investigate the factors determining α_{soil} , information about the soil cover is provided in Table 1a, b. It

is evident that no large differences exist between the Douglas fir, spruce and beech sites, i.e., the variability between sites is similar to the variability within sites. The small number of experiments impedes examining the possible small differences between sites. In order to investigate the diffusion effect, we removed the soil cover in experiments “SPU-8” and “SPU-12” at the same place of experiments “SPU-7” and “SPU-11”. The removal of leaves (“SPU-8”) and needles (“SPU-12”) increased α_{soil} by ≈ 0.014 , thus towards smaller fractionation, which indicates that diffusion contributes to the fractionation. As v_d also increases when the soil cover is removed, faster deposition is associated with smaller fractionations in these experiments, which is similar to the results from Rice et al. (2011).

The α_{soil} for the Cabauw net-uptake experiments is higher and more scattered than that for the Speuld experiments (0.951 ± 0.026 vs. 0.937 ± 0.008). This could be caused by the interference of D-depleted H₂ from the strong soil emission in Cabauw, which may not be perfectly captured via the mathematical models applied. As can be seen from the strong decline of δD with time in the middle panel of Fig. 6, though soil uptake of H₂ dominates for the Cabauw net-uptake experiments, soil production is still considerable. If part of the

source signature is not taken into account properly and appears in α_{soil} , then α_{soil} will be larger, because soil production tends to decrease δD of H₂. This could explain why α_{soil} is even larger than 1 in “CBW-7”.

The overall α_{soil} (0.945) obtained by plotting $\ln \frac{c'_1 - c'_{e,\text{app}}}{c_1 - c_{e,\text{app}}}$ vs. $\ln \frac{c - c_{e,\text{app}}}{c_1 - c_{e,\text{app}}}$ and applying the average correction factor for all the Speuld and Cabauw net-uptake experiments is similar to the results of 0.943 ± 0.024 from Gerst and Quay (2001), 0.94 ± 0.01 from Rahn et al. (2002a), and the overall α_{soil} (0.943) from Rice et al. (2011). Rice et al. (2011) suggested that the overall α_{soil} is more accurate as it is less susceptible to outliers. We argue here that the average α_{soil} of all individual experiments in Speuld (0.937) and Cabauw (0.951) is representative for a spatially averaged fractionation factor for those sites and is useful for, e.g., characterizing the phenomenon and comparing with other fractionation results. If all experiments are included in one fit, their weight for determining the slopes depends on how much H₂ has been removed, so experiments with a lower $c_{e,\text{app}}$ have a larger weight than experiments with a higher $c_{e,\text{app}}$ (i.e., experiments with a higher v_d have a larger weight than experiments with a lower v_d). The fractionation factor obtained by fitting all data together is therefore representative for a flux weighted average, which is the relevant number for the global atmospheric isotope budget.

4.3 Relationship between α_{soil} and v_d

Rice et al. (2011) proposed a significant positive correlation between α_{soil} and deposition velocity v_d in their soil uptake experiments. Figure 8 shows that no significant correlation between α_{soil} and v_d is found when considering all Speuld and Cabauw net-uptake experiments. The uptake rate is much stronger in the Speuld experiments ($v_d \approx 0.17 \text{ cm s}^{-1}$) than in the study of Rice et al. (2011) ($v_d \approx 0.04 \text{ cm s}^{-1}$), but the α_{soil} is virtually identical (0.937 vs. 0.934). Therefore, when the results from both studies are combined, the correlation reported in Rice et al. (2011) between α_{soil} and v_d disappears. We suggest that a positive correlation between α_{soil} and v_d may exist for a specific site where microbial species are similar. This was suggested from the simultaneous increase of both α_{soil} and v_d in two experiments (“SPU-8” and “SPU-12”), when soil cover was removed at the same sampling location, as mentioned in Sect. 4.2.

We conclude that there is certainly not one single correlation between α_{soil} and v_d that holds globally and the soil type might play an important role. Measurements at more sites may be needed to positively confirm whether local positive correlations between α_{soil} and v_d are common.

4.4 δD of H₂ emitted from the soil

The present study is the first field study to report δD of H₂ emitted from soils. The $\delta\text{D}_{\text{soil}}$ values (−629 to −451 ‰)

shown in Table 2 are less depleted than the H₂ in isotopic equilibrium with water (≈ -700 ‰). Previous observations from environmental H₂ production yielded a δD of −628 ‰ for two seawater samples (Rice et al., 2010), −778 ‰ for a termite headspace sample and −690 ‰ for two headspace samples from a eutrophic water pond (Rahn et al., 2002b). Kawagucci et al. (2010) proposed that microbiological H₂ consumption and production could destroy the thermal isotopic equilibrium between H₂ and H₂O in low-temperature hydrothermal fluids. Luo et al. (1991) and Walter et al. (2012) found fractionation factors of 0.448, 0.401 and 0.363 for H₂ generated from water by different N₂-fixing bacteria in the laboratory.

In order to compare our $\delta\text{D}_{\text{soil}}$ with the fractionation factors between H₂ and H₂O found by Luo et al. (1991) and Walter et al. (2012), we converted their fractionation factors to $\delta\text{D}(\text{H}_2)$ by assuming the $\delta\text{D}(\text{H}_2\text{O})$ to be the same as that of global rainwater (−37.8 ‰, Hoffmann et al., 1998). This results in $\delta\text{D}(\text{H}_2)$ values of −651 to −569 ‰ for their N₂-fixing bacteria. Although the ranges are considerable, it appears that the mean $\delta\text{D}_{\text{soil}}$ (−530 ‰) obtained in our field study is even higher than what was found for nitrogenase-derived H₂ in laboratory experiments.

It is known that H₂ produced by biogenic N₂ fixation can be largely recycled within the soil before entering the atmosphere (Evans et al., 1987; Conrad and Seiler, 1979, 1980). If this uptake process within the soil tends to increase the δD of the remaining H₂, as the soil uptake process for atmospheric H₂ does, then the H₂ entering the atmosphere will be less D depleted than pure biogenic H₂. However, if the fractionation factor of removal in the soil is similar to that determined from the net-uptake experiments (≈ 0.94), a large fraction (f_{in}) of H₂ needs to be removed in the soil before release to explain the D-enriched $\delta\text{D}_{\text{soil}}$ compared to the values reported in the literature. The fraction f_{in} could in principle be estimated from the Rayleigh equation:

$$(1 - f_{\text{in}})^{\alpha_{\text{in}} - 1} = \frac{\delta\text{D}_{\text{soil}} + 1}{\delta\text{D}_0 + 1},$$

where α_{in} is the fractionation constant of H₂ within soil, δD_0 is the δD value of initial H₂ produced by N₂-fixers, and $\delta\text{D}_{\text{soil}}$ is the δD value of remaining H₂ emitted from soil that is measured in our experiments. By assuming $\alpha_{\text{in}} = 0.945$ (overall fractionation factor as determined in our deposition experiments), $\delta\text{D}_{\text{soil}} = -530$ ‰ (averaged $\delta\text{D}_{\text{soil}}$ of Cabauw net-emission experiments) and $\delta\text{D}_0 = -611$ ‰ (averaged of $\delta\text{D}(\text{H}_2)$ derived from laboratory experiments in Luo et al. (1991) and Walter et al., 2012), we would obtain $f_{\text{in}} = 0.97$. That is, 97 % of H₂ produced by N₂ fixation would be removed within soil before entering atmosphere. This is higher than the estimate from Conrad and Seiler (1979), which was from 30 to 90 %. It should be noted that the estimation of f_{in} is very uncertain due to the lack of information about α_{in} and δD_0 . By using the lower limit of α_{in} (0.911) in our experiment and the upper limit of δD_0

(−569 ‰) in Luo et al. (1991) and Walter et al. (2012), we calculate a lower limit of f_{in} to be 0.62. The upper limit of f_{in} is 1.00 when α_{in} approaches 1. For these calculations we have used a δD_{soil} of −530 ‰, but it varies from −629 to −451 ‰ in our experiments. We cannot rule out cases with $\delta D_{soil} = \delta D_0$, which yields a f_{in} of 0.

The deuterium enrichment in the emitted H₂, compared to the value expected in isotopic equilibrium with water, could also be caused by different fractionations induced by different enzymes and/or a potentially enriched deuterium content of the substrate water available for H₂ production in Cabauw. H₂ is generated from the reduction of hydrogen ions (H⁺ or D⁺) in intracellular water (Yang et al., 2012). It was found that the isotopic composition of intracellular water can be different from that of extracellular water due to metabolic processing (Kreuzer-Martin et al., 2006). Due to the differences in H bonding and hydrogen ion transport, the fractionation may be different for different microbe species, which could result in different isotopic signatures of the produced H₂. Measurements of the isotopic composition of produced H₂ may be a tool to investigate such effects.

Finally, we note that if our Cabauw net-emission experiments are analyzed with a simple Keeling plot approach (i.e., without considering uptake), the y axis intercept is −703 ‰. We know from the temporal evolution of H₂, HD and δD that this model is not adequate and that uptake was significant in our experiments, so a simple Keeling plot analysis can be misleading if uptake is not considered.

5 Conclusions

This study investigated the isotope effects associated with the production and uptake of atmospheric H₂ by soil. Our aim was to quantify the fractionation factor α_{soil} for H₂ deposition and the isotopic signature of H₂ emitted from the soil (δD_{soil}) from experiments carried out at Speuld and Cabauw.

The experiments covered a wide range of conditions from situations with very strong net H₂ uptake to situations with very strong net H₂ emission. The superposition of deposition and production made the analysis with simple models like Rayleigh plot and Keeling plot impossible. Therefore, the mass balance model suggested by Rice et al. (2011) was used for evaluation.

The deposition velocity v_d was largest in the Speuld experiments (0.17 ± 0.02 cm s^{−1}) where also the strongest net soil uptake occurred, followed by the Cabauw net-uptake experiments (0.13 ± 0.06 cm s^{−1}) and Cabauw net-emission experiments (0.06 ± 0.03 cm s^{−1}). The net H₂ flux F_n was (-26.5 ± 4.8) nmol m^{−2} s^{−1} for Speuld experiments, (-13.6 ± 8.6) nmol m^{−2} s^{−1} for Cabauw net-uptake experiments and (49.5 ± 29.8) nmol m^{−2} s^{−1} for Cabauw net-emission experiments.

The mean fractionation factors α_{soil} are 0.937 ± 0.008 for the Speuld forest soil experiments and 0.951 ± 0.026 for the Cabauw grassland experiments, which are representative for a spatial average and useful for comparisons with other fractionation studies. The Cabauw results may be affected by the relatively strong concomitant soil emissions. The overall α_{soil} by considering all net-uptake experiments is 0.945 ± 0.004 , which is representative for a flux weighted average and useful for global isotope budget estimates. The fractionation factors found in this work are in good agreement with previous studies.

No significant correlation between α_{soil} and deposition velocity v_d was found while considering all of our experiments. The v_d were overall much larger in our study than those in Rice et al. (2011) and we obtained similar values for α_{soil} . This demonstrates that the positive correlation that was found previously does not hold globally. From two of our Speuld experiments, α_{soil} increased after the removal of leaves or needles above the soil. This indicates that there may be a fractionation associated with diffusion through the surface layer of leaves or needles during soil uptake, but more experiments are required to confirm this.

The isotopic analysis clearly showed that the net uptake was always a superposition of a larger gross uptake and a gross emission flux. In Cabauw, the emission strength was very large at locations where clover was present. Using a simple mass balance approach, the isotopic composition of the emitted H₂ was determined to be (-530 ± 40) ‰, which is significantly higher than the value expected for H₂O–H₂ isotope equilibrium. Although limited, other published data on H₂ produced biologically via nitrogenase show also a tendency to more enriched values. An additional isotope enrichment in our field soil study could originate from fractionation during the recycling of H₂ within the soil before it enters the atmosphere.

Appendix A

A1 Flask sampling model

A mathematical model is used to simulate the sampling and to correct for the effects of the flask sampling method on the values of uptake rate constant (k), production rate (P), fractionation factor (α_{soil}) and isotopic signature of H₂ produced from soil (δD_{soil}). We start with a pair of known (true) uptake and production rates and simulate the evolution of the mole fractions of H₂ and HD in the flasks and chamber. From the modeled mole fractions we calculate the apparent uptake and production rates and derive the correction needed to obtain the true uptake and production rates from measurement of the apparent rates in actual experiments.

A1.1 Mathematical description of the flask sampling model

The sampling setup is shown in Fig. 2 of the main paper. After 10 min of flushing, the chamber and the flasks contain ambient air with the prevailing H₂ and HD mole fractions. In the following we denote $c_1(t)$, $c_2(t)$, $c_3(t)$, $c_4(t)$ and $c_0(t)$ the H₂ mole fractions for the first, second, third and fourth flask and the chamber, respectively. The moment when the first flask and the chamber lid are closed is considered the starting time of the experiment ($t = 0$). From this point on, only the chamber and the second, third and fourth flask are connected, and the initial H₂ mole fraction inside them is $c_0(0) = c_2(0) = c_3(0) = c_4(0) = c_1$. We start a simulation with an input uptake rate constant (k_{true}) and an input production rate (P_{true}). The simulation of the flask sampling is based on Eqs. (A1)–(A4) shown below.

Assuming that the air in each flask and in the chamber is well mixed during the entire sampling process, the time evolution for the second flask $c_2(t)$, third flask $c_3(t)$, fourth flask $c_4(t)$ and the chamber $c_0(t)$ in the first 10 min after starting the experiment can be expressed as

$$\frac{dc_2(t)}{dt} = \frac{f}{V}c_0(t) - \frac{f}{V}c_2(t), \quad (\text{A1})$$

$$\frac{dc_3(t)}{dt} = \frac{f}{V}c_2(t) - \frac{f}{V}c_3(t), \quad (\text{A2})$$

$$\frac{dc_4(t)}{dt} = \frac{f}{V}c_3(t) - \frac{f}{V}c_4(t), \quad (\text{A3})$$

$$\frac{dc_0(t)}{dt} = \frac{f}{V'}c_4(t) - \frac{f}{V'}c_0(t) + (P_{\text{true}} - k_{\text{true}}c_0(t)), \quad (\text{A4})$$

where V and V' are the air volumes of the flask and chamber, and f is the flow rate. These differential equations are solved using the Matlab ODE solvers at time steps of 0.01 min. The input parameters are $c_0(0)$, P_{true} , k_{true} , V , V' and f . For each time step the solvers calculate the hydrogen flux into and out of the chamber and each flask, as well as the new mole fractions there.

After 10 min, the second flask is closed and now contains air with mole fraction $c_2 = c_2(10 \text{ min})$. From this point on, only the chamber, the third and the fourth flask are connected, and the time evolution of the mole fractions can be expressed as

$$\frac{dc_3(t)}{dt} = \frac{f}{V}c_0(t) - \frac{f}{V}c_3(t), \quad (\text{A5})$$

$$\frac{dc_4(t)}{dt} = \frac{f}{V}c_3(t) - \frac{f}{V}c_4(t), \quad (\text{A6})$$

$$\frac{dc_0(t)}{dt} = \frac{f}{V'}c_4(t) - \frac{f}{V'}c_0(t) + (P_{\text{true}} - k_{\text{true}}c_0(t)). \quad (\text{A7})$$

After another 10 min of sampling, the third flask is closed $c_3 = c_3(20 \text{ min})$, and only the chamber and the fourth flask are connected. Then, the time evolution for the fourth flask and the chamber can be expressed as

$$\frac{dc_4(t)}{dt} = \frac{f}{V}c_0(t) - \frac{f}{V}c_4(t), \quad (\text{A8})$$

$$\frac{dc_0(t)}{dt} = \frac{f}{V'}c_4(t) - \frac{f}{V'}c_0(t) + (P_{\text{true}} - k_{\text{true}}c_0(t)). \quad (\text{A9})$$

The H₂ mole fraction inside the chamber and the fourth flask at time $t = 30 \text{ min}$ is $c_0(30)$ and $c_4(30)$.

In the end, a set of four flasks with mole fractions $c_1(0)$, $c_2(10 \text{ min})$, $c_3(20 \text{ min})$ and $c_4(30 \text{ min})$ is obtained. By fitting this set of four data points with an exponential function $c = ae^{-k_{\text{app}}t} + c_{e,\text{app}}$ (see Eq. 2 in the main paper), we can obtain the apparent soil uptake rate constant (k_{app}) and equilibrium concentration ($c_{e,\text{app}}$) and further calculate apparent production rate ($P_{\text{app}} = k_{\text{app}}c_{e,\text{app}}$). These apparent rates k_{app} and P_{app} are different from the assumed true rates k_{true} and P_{true} . The flask sampling model enables us to establish a relation between k_{app} and P_{app} and k_{true} and P_{true} , so that k_{true} and P_{true} can be derived from k_{app} and P_{app} in actual experiments, where the true values are unknown. To accomplish this, simulations are carried out with a wide range of values for k_{true} and P_{true} , and a corresponding data set of k_{app} and P_{app} is generated. Similarly, we use a new set of input uptake rate constant k'_{true} and production rate P'_{true} for HD and generate a corresponding data set of k'_{app} and P'_{app} .

A1.2 The correction coefficients for k and P

Here we discuss an example of the relationship between k_{true} and k_{app} for the setup used in some Cabauw experiments ($V' = 22.8 \text{ L}$, $f = 2 \text{ L min}^{-1}$ and $\Delta t = 10 \text{ min}$). The pressure inside the flasks is 200 kPa and the pressure inside the chamber is 100 kPa. The relationship between $k_{\text{true}} / k_{\text{app}}$ and k_{app} is shown in Fig. 10a. The ratio $k_{\text{true}} / k_{\text{app}}$ varies between 1.45 to 1.61 for our k_{app} range of 0.04 to 0.30 min^{-1} . This relationship does not depend on P_{true} (with P_{true} varying from 50 to 650 ppb min^{-1}). An additional uncertainty can arise from incorrect timing of the flask sampling, but sampling times should be correct within few seconds, which may lead to an additional uncertainty of below 1 %. The uncertainty of the

flow rate obtained from the rotameter due to variations in ambient pressure and temperature that were not recorded is less than 4 %, and the effect on the ratio $k_{\text{true}}/k_{\text{app}}$ ratio is below 1 %. We can retrieve k_{true} by multiplying k_{app} with the modeled value of $k_{\text{true}}/k_{\text{app}}$ for each experiment. The ratio $k_{\text{true}}/k_{\text{app}}$ for each experiment is shown in Table 3. It depends on experimental setup and k_{app} of each experiment, with a range of 1.177 to 1.589.

After retrieving k_{true} from k_{app} , we investigate the relationship between $P_{\text{true}}/P_{\text{app}}$ and P_{app} for a fixed value of k_{true} (Fig. 10b). The ratio $P_{\text{true}}/P_{\text{app}}$ depends slightly on P_{app} and k_{true} , ranging from 1.40 to 1.59 for a wide P_{app} range of 30 to 450 ppb min⁻¹ and a wide k_{true} range of 0.05 to 0.45 min⁻¹. As for the correction of k , uncertainties arising from incorrect timing of the flask sampling and from pressure and temperature variations and their effect on the flow rate lead to additional uncertainties of $P_{\text{true}}/P_{\text{app}}$ ratio below 1 %, which are not considered. We can retrieve P_{true} by multiplying P_{app} with $P_{\text{true}}/P_{\text{app}}$ for each experiment after having determined k_{true} from k_{app} . The ratio $P_{\text{true}}/P_{\text{app}}$ for each experiment is shown in Table 3 and depends on the experimental setup, P_{app} and k_{app} of each experiment. It ranges from 1.152 to 2.759 for most experiments, with an exception of 7.472 for experiment SPU-2 where a very small P_{app} of 0.67 ppb min⁻¹ is found. Although the ratio $P_{\text{true}}/P_{\text{app}}$ of experiment SPU-2 is high, P_{true} of SPU-2 is still smaller than the rest of the experiments. $P_{\text{true}}/P_{\text{app}}$ ratios for experiments SPU-10 and SPU-11 are null because these two experiments show a P_{app} of 0.

A1.3 The correction coefficients for α_{soil} and δD_{soil}

In our experiments, the uncertainties of k_{app} and k'_{app} derived from exponential fits to the time evolution of HH and HD are rather large, which results in a large scatter of $\alpha_{\text{soil,app}}$ if $\alpha_{\text{soil,app}}$ is calculated directly as $k'_{\text{app}}/k_{\text{app}}$. Thus, we obtained $\alpha_{\text{soil,app}}$ by plotting $\ln \frac{c' - c'_{\text{e,app}}}{c'_1 - c'_{\text{e,app}}}$ vs. $\ln \frac{c - c_{\text{e,app}}}{c_1 - c_{\text{e,app}}}$ (Fig. 7) for each experiment which yields a smaller scatter for $\alpha_{\text{soil,app}}$.

Correction coefficients to convert $\alpha_{\text{soil,app}}$ to $\alpha_{\text{soil,true}}$ are obtained using the flask sampling model by comparing $\alpha_{\text{soil,true}}$ used as input for the model run to $\alpha_{\text{soil,app}}$ derived from the plot of $\ln \frac{c' - c'_{\text{e,app}}}{c'_1 - c'_{\text{e,app}}}$ vs. $\ln \frac{c - c_{\text{e,app}}}{c_1 - c_{\text{e,app}}}$ of the output values, like in the experiments. Figure 10c shows $\alpha_{\text{soil,true}}/\alpha_{\text{soil,app}}$ as a function of $\alpha_{\text{soil,app}}$ for a wide $\delta D_{\text{soil,true}}$ range of -750 to -250 ‰ with the sampling setup described above ($V' = 22.8 \text{ L}$, $f = 2 \text{ L min}^{-1}$ and $\Delta t = 10 \text{ min}$) for $k_{\text{true}} = 0.25 \text{ min}^{-1}$ and $P_{\text{true}} = 50 \text{ ppb min}^{-1}$. In this case the correction factor $\alpha_{\text{soil,true}}/\alpha_{\text{soil,app}}$ varies from 0.98 to 1.00 for a $\alpha_{\text{soil,app}}$ range of 0.90 to 1.00, and it does not depend on $\delta D_{\text{soil,true}}$. Thus, after retrieving k_{true} and P_{true} as described in Sect. A1.2, we can retrieve $\alpha_{\text{soil,true}}$ from $\alpha_{\text{soil,app}}$ for

each experiment. The correction factors range from 0.984 to 1.007, depending on the experimental setup and $\alpha_{\text{soil,app}}$ of each experiment (Table 3).

Similarly, in our experiments, the uncertainties of P_{app} and P'_{app} derived from exponential fits of time evolution of HH and HD are large, which results in a large scatter of $\delta D_{\text{soil,app}}$ if $\delta D_{\text{soil,app}}$ is calculated directly from these P'_{app} and P_{app} . We therefore obtained the ratio $P'_{\text{app}}/P_{\text{app}}$ by plotting $c'_{\text{e,app}} \ln \frac{c' - c'_{\text{e,app}}}{c'_1 - c'_{\text{e,app}}}$ vs. $c_{\text{e,app}} \ln \frac{c - c_{\text{e,app}}}{c_1 - c_{\text{e,app}}}$ (Fig. 9) and calculated $\delta D_{\text{soil,app}}$ from Eq. (4). This yielded smaller scatter for $\delta D_{\text{soil,app}}$. After retrieving k_{true} , P_{true} and $\alpha_{\text{soil,true}}$ as described above, we used the flask sampling model again to derive correction factors by comparing $\delta D_{\text{soil,true}}$ used as model input with $\delta D_{\text{soil,app}}$ obtained from $c'_{\text{e,app}} \ln \frac{c' - c'_{\text{e,app}}}{c'_1 - c'_{\text{e,app}}}$ vs. $c_{\text{e,app}} \ln \frac{c - c_{\text{e,app}}}{c_1 - c_{\text{e,app}}}$ of the model output and to retrieve $\delta D_{\text{soil,true}}$ from $\delta D_{\text{soil,app}}$ for each experiment. Figure 10d shows $(\delta D_{\text{soil,true}} + 1) / (\delta D_{\text{soil,app}} + 1)$ as a function of $(\delta D_{\text{soil,app}} + 1)$ for a $\alpha_{\text{soil,true}}$ range of 0.90 to 1.00 with the sampling setup described above ($V' = 22.8 \text{ L}$, $f = 2 \text{ L min}^{-1}$ and $\Delta t = 10 \text{ min}$) for $k_{\text{true}} = 0.25 \text{ min}^{-1}$ and $P_{\text{true}} = 50 \text{ ppb min}^{-1}$. The ratio $(\delta D_{\text{soil,true}} + 1) / (\delta D_{\text{soil,app}} + 1)$ changes from 0.99 to 1.05 for a wide $(\delta D_{\text{soil,app}} + 1)$ range of 0.25 to 0.65. It can be seen that the $(\delta D_{\text{soil,true}} + 1) / (\delta D_{\text{soil,app}} + 1)$ ratio depends slightly on $\alpha_{\text{soil,true}}$ at a fixed $(\delta D_{\text{soil,app}} + 1)$, with a maximum difference of about 1 % for a $\alpha_{\text{soil,true}}$ range of 0.90 to 1.00. The ratio $(\delta D_{\text{soil,true}} + 1) / (\delta D_{\text{soil,app}} + 1)$ for each net-emission experiment is shown in Table 3, ranging from 1.007 to 1.048. The largest difference between $\delta D_{\text{soil,true}}$ and $\delta D_{\text{soil,app}}$ is 21 ‰ for CBW-8. The mean δD_{true} and δD_{app} for these net-emission experiments are -530 and -538 ‰, respectively.

In conclusion, the effect of the flask sampling process is relatively small for α_{soil} and δD_{soil} but considerable for the uptake rate constants k and k' and emission rates P and P' . The flask sampling model allows us to derive corresponding corrections that have been applied to correct for the bias introduced by the flask sampling system.

Acknowledgements. We are grateful to C. Van der Veen, M. Bolder and H. Snellen for their help maintaining the GC-IRMS system and setup of the sampling. We are also grateful to Jan Kaiser for giving valuable comments on the flask sampling model. This work was supported by the Netherlands Organisation for Scientific Research (NWO) as part of the NWO-ACTS Sustainable Hydrogen (H₂) project 2007/00566/ACTS, grant numbers 053.61.026 and 053.61.126.

Edited by: J. Kaiser

References

- Batenburg, A. M., Walter, S., Pieterse, G., Levin, I., Schmidt, M., Jordan, A., Hammer, S., Yver, C., and Röckmann, T.: Temporal and spatial variability of the stable isotopic composition of atmospheric molecular hydrogen: observations at six EUROHYDROS stations, *Atmos. Chem. Phys.*, 11, 6985–6999, doi:10.5194/acp-11-6985-2011, 2011.
- Beljaars, A. C. M. and Bosveld, F. C.: Cabauw data for the validation of land surface parameterization schemes, *J. Climate*, 10, 1172–1193, doi:10.1175/1520-0442(1997)010<1172:CDFTVO>2.0.CO;2, 1997.
- Belnap, J.: Factors influencing nitrogen fixation and nitrogen release in biological soil crusts, Springer-Verlag, Berlin, Heidelberg, 241–261, 2001.
- Bottinga, Y.: Calculated fractionation factors for carbon and hydrogen isotope exchange in the system calcite-carbon dioxide-graphite-methane-hydrogen-water vapour, *Geochim. Cosmochim. Ac.*, 33, 49–64, doi:10.1016/0016-7037(69)90092-1, 1969.
- Conrad, R.: Compensation concentration as critical variable for regulating the flux of trace gases between soil and atmosphere, *Bio-geochemistry*, 27, 155–170, doi:10.1007/BF00000582, 1994.
- Conrad, R. and Seiler W.: Field measurements of hydrogen evolution by nitrogen-fixing legumes, *Soil Biol. Biochem.*, 11, 689–690, doi:10.1016/0038-0717(79)90041-5, 1979.
- Conrad, R. and Seiler, W.: Contribution of hydrogen production by biological nitrogen fixation to the global hydrogen budget, *J. Geophys. Res.*, 85, 5493–5498, doi:10.1029/JC085iC10p05493, 1980.
- Conrad, R. and Seiler, W.: Decomposition Of atmospheric hydrogen by soil microorganisms and soil enzymes, *Soil Biol. Biochem.*, 13, 43–49, doi:10.1016/0038-0717(81)90101-2, 1981.
- Conrad, R. and Seiler, W.: Influence of temperature, moisture, and organic carbon on the flux of H₂ and CO between soil and atmosphere: field studies in subtropical regions, *J. Geophys. Res.*, 90, 5699–5709, doi:10.1029/JD090iD03p05699, 1985.
- Conrad, R., Weber, M., and Seiler, W.: Kinetics and electron transport of soil hydrogenases catalyzing the oxidation of atmospheric hydrogen, *Soil Biol. Biochem.*, 15, 167–173, doi:10.1016/0038-0717(83)90098-6, 1983.
- Constant, P., Poissant, L., and Villemur, R.: Isolation of *Streptomyces* sp. PCB7, the first microorganism demonstrating high-affinity uptake of tropospheric H₂, *ISME J.*, 2, 1066–1076, doi:10.1038/ismej.2008.59, 2008a.
- Constant, P., Poissant, L., and Villemur, R.: Annual hydrogen, carbon monoxide and carbon dioxide concentrations and surface to air exchanges in a rural area (Québec, Canada), *Atmos. Environ.*, 42, 5090–5100, doi:10.1016/j.atmosenv.2008.02.021, 2008b.
- Constant, P., Chowdhury, S. P., Pratscher, J., and Conrad, R.: *Streptomyces* contributing to atmospheric molecular hydrogen soil uptake are widespread and encode a putative high-affinity [NiFe]-hydrogenase, *Environ. Microbiol.*, 12, 821–829, doi:10.1111/j.1462-2920.2009.02130.x, 2010.
- Constant, P., Chowdhury, S. P., Hesse, L., and Conrad, R.: Co-localization of atmospheric H₂ oxidation activity and high affinity H₂-oxidizing bacteria in non-axenic soil and sterile soil amended with *Streptomyces* sp. PCB7, *Soil Biol. Biochem.*, 43, 1888–1893, doi:10.1016/j.soilbio.2011.05.009, 2011.
- De Wit, J. C., Van der Straten, C. M., and Mook, W. G.: Determination of the absolute isotopic ratio of V-SMOW and SLAP, *Geostandard. Newslett.*, 4, 33–36, doi:10.1111/j.1751-908X.1980.tb00270.x, 1980.
- Ehhalt, D. H. and Rohrer, F.: The tropospheric cycle of H₂: a critical review, *Tellus B*, 61, 500–535, doi:10.1111/j.1600-0889.2009.00416.x, 2009.
- Ehhalt, D. H. and Rohrer, F.: The dependence of soil H₂ uptake on temperature and moisture: a reanalysis of laboratory data, *Tellus B*, 63, 1040–1051, doi:10.1111/j.1600-0889.2011.00581.x, 2011.
- Ehhalt, D. H. and Rohrer, F.: Deposition velocity of H₂: a new algorithm for its dependence on soil moisture and temperature, *Tellus B*, 65, 19904, doi:10.3402/tellusb.v65i0.19904, 2013a.
- Ehhalt, D. H. and Rohrer, F.: Dry deposition of molecular hydrogen in the presence of H₂ production, *Tellus B*, 65, 20620, doi:10.3402/tellusb.v65i0.20620, 2013b.
- Evans, H. J., Harker, A. R., Papen, H., Russell, S. A., Hanus, F. J., and Zuber, M.: Physiology, biochemistry, and genetics of the uptake hydrogenase in rhizobia, *Annu. Rev. Microbiol.*, 41, 335–361, 1987.
- Gerst, S. and Quay, P.: The deuterium content of atmospheric molecular hydrogen: Method and initial measurements, *J. Geophys. Res.*, 105, 26433–26445, doi:10.1029/2000JD900387, 2000.
- Gerst, S. and Quay, P.: Deuterium component of the global molecular hydrogen cycle, *J. Geophys. Res.*, 106, 5021–5031, doi:10.1029/2000JD900593, 2001.
- Förstel, H.: HT to HTO conversion in the soil and subsequent tritium pathway: field release data and laboratory experiments, *Fusion Technol.*, 14, 1241–1246, 1988.
- Förstel, H. and Führ, F.: Trockene Deposition von Tritium in den Boden, Annual Report, Forschungszentrum Jülich, Jülich, 45–51, 1992.
- Gonfiantini, R., Stichler, W., and Rozanski, K.: Standards and intercomparison materials distributed by the International Atomic Energy Agency for stable isotope measurements, in: Reference and intercomparison materials for stable isotopes of light elements: Proceedings of a consultants meeting held in Vienna, 1–3 December 1993, IAEA-TECDOC-825, International Atomic Energy Agency, Vienna, 1993.
- Guo, R. and Conrad, R.: Extraction and characterization of soil hydrogenases oxidizing atmospheric hydrogen, *Soil Biol. Biochem.*, 40, 1149–1154, doi:10.1016/j.soilbio.2007.12.007, 2008.
- Häring, V., Klüber, H. D., and Conrad, R.: Localization of atmospheric H₂-oxidizing soil hydrogenases in different

- particle fractions of soil, *Biol. Fert. Soils*, 18, 109–114, doi:10.1007/BF00336455, 1994.
- Haumann, F. A., Batenburg, A. M., Pieterse, G., Gerbig, C., Krol, M. C., and Röckmann, T.: Emission ratio and isotopic signatures of molecular hydrogen emissions from tropical biomass burning, *Atmos. Chem. Phys.*, 13, 9401–9413, doi:10.5194/acp-13-9401-2013, 2013.
- Heij, G. H. and Erisman, J. W.: Acid Atmospheric Deposition and Its Effects on Terrestrial Ecosystems in The Netherlands, *Studies in Environmental Sciences* 69, ISBN 0-444-82037-X, Elsevier, Amsterdam, 1997.
- Hoffmann, G., Werner, M., and Heimann, M.: The water isotope module of the ECHAM atmospheric general circulation model – A study on the time scales from days to several years, *J. Geophys. Res.*, 103, 16871–16896, doi:10.1029/98JD00423, 1998.
- Jordan, A. and Steinberg, B.: Calibration of atmospheric hydrogen measurements, *Atmos. Meas. Tech.*, 4, 509–521, doi:10.5194/amt-4-509-2011, 2011.
- Kawagucci, S., Toki, T., Ishibashi, J., Takai, K., Ito, M., Oomori, T., and Gamo, T.: Isotopic variation of molecular hydrogen in 20°–375 °C hydrothermal fluids as detected by a new analytical method, *J. Geophys. Res.*, 115, G03021, doi:10.1029/2009JG001203, 2010.
- Khdhiri, M., Hesse, L., Popa, M. E., Quiza, L., Lalonde, I., Meredith, L. K., Röckmann, T., and Constant, P.: Soil carbon content and relative abundance of high affinity H₂-oxidizing bacteria predict atmospheric H₂ soil uptake activity better than soil microbial community composition, *Soil Biol. Biochem.*, 85, 1–9, doi:10.1016/j.soilbio.2015.02.030, 2015.
- Kreuzer-Martin, H. W., Lott, M. J., Ehleringer, J. R., and Hegg, E. L.: Metabolic processes account for the majority of the intracellular water in log-phase *Escherichia coli* cells as revealed by hydrogen isotopes, *Biochemistry*, 45, 13622–13630, doi:10.1021/bi0609164, 2006.
- Luo, Y., Sternberg, L., Suda, S., Kmazawa, S., and Mitsui, A.: Extremely low D/H ratios of photoproduct hydrogen by cyanobacteria, *Plant Cell Physiol.*, 32, 897–900, 1991.
- Meredith, L. K.: Field measurement of the fate of atmospheric H₂ in a Forest environment: from canopy to soil, Ph.D. thesis, Department of Earth, Atmospheric and Planetary Sciences, Massachusetts Institute of Technology, USA, 250 pp., 2012.
- Novelli, P. C., Lang, P. M., Masarie, K. A., Hurst, D. F., Myers, R., and Elkins, J. W.: Molecular hydrogen in the troposphere: Global distribution and budget, *J. Geophys. Res.*, 104, 30427–30444, doi:10.1029/1999JD900788, 1999.
- Pieterse, G., Krol, M. C., Batenburg, A. M., Steele, L. P., Krummel, P. B., Langenfelds, R. L., and Röckmann, T.: Global modelling of H₂ mixing ratios and isotopic compositions with the TM5 model, *Atmos. Chem. Phys.*, 11, 7001–7026, doi:10.5194/acp-11-7001-2011, 2011.
- Pieterse, G., Krol, M. C., Batenburg, A. M., Brenninkmeijer, C. A. M., Popa, M. E., O'Doherty, S., Grant, A., Steele, L. P., Krummel, P. B., Langenfelds, R. L., Wang, H. J., Vermeulen, A. T., Schmidt, M., Yver, C., Jordan, A., Engel, A., Fisher, R. E., Lowry, D., Nisbet, E. G., Reimann, S., Vollmer, M. K., Steinbacher, M., Hammer, S., Forster, G., Sturges, W. T., and Röckmann, T.: Reassessing the variability in atmospheric H₂ using the two-way nested TM5 model, *J. Geophys. Res.-Atmos.*, 118, 3764–3780, doi:10.1002/jgrd.50204, 2013.
- Popa, M. E., Vermeulen, A. T., van den Bulk, W. C. M., Jongejan, P. A. C., Batenburg, A. M., Zahorowski, W., and Röckmann, T.: H₂ vertical profiles in the continental boundary layer: measurements at the Cabauw tall tower in The Netherlands, *Atmos. Chem. Phys.*, 11, 6425–6443, doi:10.5194/acp-11-6425-2011, 2011.
- Price, H., Jaeglé, L., Rice, A., Quay, P., Novelli, P. C., and Gammon, R.: Global budget of molecular hydrogen and its deuterium content: Constraints from ground station, cruise, and aircraft observations, *J. Geophys. Res.-Atmos.*, 112, D22108, doi:10.1029/2006JD008152, 2007.
- Rahn, T., Eiler, J. M., Kitchen, N., Fessenden, J. E., and Randerson, J. T.: Concentration and δD of molecular hydrogen in boreal forests: Ecosystem-scale systematics of atmospheric H₂, *Geophys. Res. Lett.*, 29, 35-1–35-4, doi:10.1029/2002GL015118, 2002a.
- Rahn, T., Kitchen, N., and Eiler, J.: D/H ratios of atmospheric H₂ in urban air: results using new methods for analysis of nanomolar H₂ samples, *Geochim. Cosmochim. Ac.*, 66, 2475–2481, doi:10.1016/S0016-7037(02)00858-X, 2002b.
- Rahn, T., Eiler, J. M., Boering, K. A., Wennberg, P. O., McCarthy, M. C., Tyler, S., Schauffler, S., Donnelly, S., and Atlas, E.: Extreme deuterium enrichment in stratospheric hydrogen and the global atmospheric budget of H₂, *Nature*, 424, 918–921, doi:10.1038/nature01917, 2003.
- Rahn, T., Randerson, J. T., and Eiler, J.: Variability of Deuterium Fractionation Associated With Soil Uptake of Atmospheric Molecular Hydrogen, *Eos Trans. AGU*, 86(52), Fall Meet. Suppl., Abstract B11A-1031, 2005.
- Rhee, T. S., Mak, J., Röckmann, T., and Brenninkmeijer, C. A. M.: Continuous-flow isotope analysis of the deuterium/hydrogen ratio in atmospheric hydrogen, *Rapid Commun. Mass Sp.*, 18, 299–306, doi:10.1002/rcm.1309, 2004.
- Rice, A., Quay, P., Stutsman, J., Gammon, R., Price, H., and Jaeglé, L.: Meridional distribution of molecular hydrogen and its deuterium content in the atmosphere, *J. Geophys. Res.*, 115, D12306, doi:10.1029/2009JD012529, 2010.
- Rice, A., Dayalu, A., Quay, P., and Gammon, R.: Isotopic fractionation during soil uptake of atmospheric hydrogen, *Biogeochemistry*, 8, 763–769, doi:10.5194/bg-8-763-2011, 2011.
- Röckmann, T., Rhee, T. S., and Engel, A.: Heavy hydrogen in the stratosphere, *Atmos. Chem. Phys.*, 3, 2015–2023, doi:10.5194/acp-3-2015-2003, 2003a.
- Röckmann, T., Kaiser, J., Brenninkmeijer, C. A. M., and Brand, W. A.: Gas chromatography/isotope-ratio mass spectrometry method for high-precision position-dependent ¹⁵N and ¹⁸O measurements of atmospheric nitrous oxide, *Rapid Commun. Mass Sp.*, 17, 1897–1908, 2003b.
- Röckmann, T., Álvarez, C. X. G., Walter, S., Veen, C. van der, Wollny, A. G., Gunthe, S. S., Helas, G., Pöschl, U., Keppler, F., Greule, M., and Brand, W. A.: Isotopic composition of H₂ from wood burning: Dependency on combustion efficiency, moisture content, and δD of local precipitation, *J. Geophys. Res.*, 115, D17308, doi:10.1029/2009JD013188, 2010.
- Rothe, M., Jordan, A., and Brand, W. A.: Trace gases, $\delta^{13}C$ and $\delta^{18}O$ of CO₂-in-air samples: Storage in glass flasks using PCTFE seals and other effects, in: GAW report 161, 12th WMO/IAEA meeting of experts on carbon dioxide concentration and related tracers measurements techniques, edited by: Wor-

- thy, D. and Huang, L., Toronto, Canada, 15–18 September 2003, WMO TD No. 1275, 2004.
- Schmitt, S., Hanselmann, A., Wollschläger, U., Hammer, S., and Levin, I.: Investigation of parameters controlling the soil sink of atmospheric molecular hydrogen, *Tellus B*, 61, 416–423, 2009.
- Schultz, M. G., Diehl, T., Brasseur, G. P., and Zittel, W.: Air pollution and climate-forcing impacts of a global hydrogen economy, *Science*, 302, 624–627, doi:10.1126/science.1089527, 2003.
- Smith-Downey, N. V., Randerson, J. T., and Eiler, J. M.: Temperature and moisture dependence of soil H₂ uptake measured in the laboratory, *Geophys. Res. Lett.*, 33, L14813, doi:10.1029/2006GL026749, 2006.
- Smith-Downey, N. V., Randerson, J. T., and Eiler, J. M.: Molecular hydrogen uptake by soils in forest, desert, and marsh ecosystems in California, *J. Geophys. Res.-Biogeo.*, 113, G03037, doi:10.1029/2008JG000701, 2008.
- Tromp, T. K., Shia, R. L., Allen, M., Eiler, J. M., and Yung, Y. L.: Potential environmental impact of a hydrogen economy on the stratosphere, *Science*, 300, 1740–1742, doi:10.1126/science.1085169, 2003.
- Vogel, B., Feck, T., Groß, J. U., and Riese, M.: Impact of a possible future global hydrogen economy on Arctic stratospheric ozone loss, *Energ. Environ. Sci.*, 5, 6445–6452, doi:10.1039/c2ee03181g, 2012.
- Vollmer, M. K., Walter, S., Mohn, J., Steinbacher, M., Bond, S. W., Röckmann, T., and Reimann, S.: Molecular hydrogen (H₂) combustion emissions and their isotope (D/H) signatures from domestic heaters, diesel vehicle engines, waste incinerator plants, and biomass burning, *Atmos. Chem. Phys.*, 12, 6275–6289, doi:10.5194/acp-12-6275-2012, 2012.
- Van Ruijven, B., Lamarque, J. F., Van Vuuren, D. P., Kram, T., and Eerens, H.: Emission scenarios for a global hydrogen economy and the consequences for global air pollution, *Global Environ. Chang.*, 21, 983–994, 2011.
- Walter, S., Laukenmann, S., Stams, A. J. M., Vollmer, M. K., Gleixner, G., and Röckmann, T.: The stable isotopic signature of biologically produced molecular hydrogen (H₂), *Biogeochemistry*, 9, 4115–4123, doi:10.5194/bg-9-4115-2012, 2012.
- Warwick, N. J., Bekki, S., Nisbet, E. G., and Pyle, J. A.: Impact of a hydrogen economy on the stratosphere and troposphere studied in a 2-D model, *Geophys. Res. Lett.*, 31, 2–5, doi:10.1029/2003GL019224, 2004.
- Xiao, X., Prinn, R. G., Simmonds, P. G., Steele, L. P., Novelli, P. C., Huang, J., Langenfelds, R. L., O'Doherty, S., Krummel, P. B., Fraser, P. J., Porter, L. W., Weiss, R. F., Salameh, P., and Wange, R. H. J.: Optimal estimation of the soil uptake rate of molecular hydrogen from the Advanced Global Atmospheric Gases Experiment and other measurements, *J. Geophys. Res.*, 112, D07303, doi:10.1029/2006JD007241, 2007.
- Yang, H., Gandhi, H., Shi, L., Kreuzer, H. W., Ostrom, N. E., and Hegg, E. L.: Using gas chromatography/isotope ratio mass spectrometry to determine the fractionation factor for H₂ production by hydrogenases, *Rapid Commun. Mass Sp.*, 26, 61–68, doi:10.1002/rcm.5298, 2012.